ORIGINAL RESEARCH ARTICLE

Temperature Dependence of the γ/γ' Interfacial Energy in Binary Ni–Al Alloys

ALAN J. ARDELL

Published data on the coarsening kinetics of γ' (Ni_3Al) precipitates in binary Ni–Al alloys aged at 12 temperatures ranging from 773 K to 1073 K are analyzed to provide a comprehensive evaluation of the temperature dependence of the γ/γ' interfacial free energy, σ. The data are analyzed using equations of the trans-interface-diffusion-controlled (TIDC) theory of coarsening, with temporal exponent $n = 2.4$. The results show that σ decreases with increasing temperature, T. A linear empirical equation is fitted to the data on σ *vs* T; it extrapolates to $\sigma = 0$ in the liquid region of the Ni–Al phase diagram, as it should do. A quantitative temperature-dependent transition radius, r_{trans}, is calculated; it depends on the product of the interface width and the ratio of the chemical diffusion coefficients in the γ phase and interface regions. Applying the TIDC coarsening equations to calculate σ is justified when the average radius, $\langle r \rangle$, satisfies the condition $\langle r \rangle < r_{trans}$, which is valid for all the data used in the fit. The data on σ *vs* T are compared with theoretical predictions. The results are discussed in the context of previous work, as well as with values of σ obtained through analyses using the equations of traditional LSW coarsening kinetics, $n = 3$.

https://doi.org/10.1007/s11661-021-06440-0

I. INTRODUCTION

THE γ' (Ni_3Al) phase in binary Ni–Al alloys is the forebear of the multicomponent γ' phases responsible for the high strength of today's commercial Ni-based superalloys, and in many cases newly developing Co-based superalloys and high-entropy alloys. Its importance has engendered a myriad of investigations, including the kinetics of γ' precipitation from supersaturated solid solution, thermodynamic assessments of the Ni–Al phase diagram, strengthening at ambient and elevated temperatures of two-phase $\gamma + \gamma'$ alloys, as well as phase-field and atomistic modeling and physical property measurements of both the disordered γ (Ni–Al) solid solution and ordered γ' phases. Reliable values of nearly every important physical and thermodynamic parameter, including their compositional and temperature dependencies, can be found in the archival literature. A major exception is the temperature dependence of the interfacial free energy (IFE), σ, of the coherent γ–γ' interface. Unfortunately, there is no σ-meter that enables its direct physical measurement experimentally, leaving us with two options: 1. Estimation of σ from atomistic and/or thermodynamic modeling and 2. the extraction of trustworthy values of σ from experimental measurements of the kinetics of γ' precipitate coarsening conducted over a range of temperatures.

Each option has its advantages and disadvantages. Atomistic models invariably simulate the atomic structures across specific low-index crystallographic planes, leading to predictions of anisotropic IFEs. Thermodynamic models, on the other hand, do not take crystallography into account, but calculate the IFE from knowledge of the Gibbs free energies of the bulk phases flanking the interface and the free energy of the interface itself. All the models predict that σ decreases slowly with increasing temperature, T, but to date there have been only two reports of experimental data on σ *vs* T, one by Marsh and Chen[1] and the other by the author[2]; both investigations utilized data on the kinetics of coarsening of the γ' precipitates at various temperatures. Not only are both sets of data incomplete, but the methods of analysis differ significantly.

The objective of the work reported in this paper is to examine all the extant published data on particle coarsening that can be analyzed within the framework of theories of matrix-diffusion-controlled (MDC) and trans-interface-diffusion-controlled (TIDC) coarsening behavior. MDC coarsening is exemplified by the seminal theory of Lifshitz and Slyozov[3] and Wagner[4] (LSW) and TIDC coarsening is exemplified by the theory of Ardell and Ozolins.[5] During coarsening four physical quantities inevitably vary as a function of time, t: 1. The average radius $\langle r \rangle$ of the polydisperse assembly of γ'

ALAN J. ARDELL is with the Department of Materials Science and Engineering, UCLA Samueli School of Engineering, University of California, Los Angeles, Los Angeles, CA 90095-1595. Contact e-mail: aardell@ucla.edu

Manuscript submitted June 12, 2021; accepted August 18, 2021.
Article published online September 29, 2021

precipitates; 2. The concentration of Al in the γ matrix phase, X_γ ; 3. The γ' volume fraction, f; and 4. The number of particles per unit volume (the number density), N_v. In order to extract trustworthy values of σ without input from data on diffusion in the γ phase, any particular set of published data must include data on the kinetics of particle growth plus data on the kinetics of solute depletion, the kinetics of volume fraction augmentation, or the kinetics of particle evanescence (the ultimate decrease of N_v with t). The concentration of Al in the γ' phase, $X_{\gamma'}$, also varies with t, but is unimportant in the context of this paper.

The paper is organized as follows. The background equations required for the analyses of experimental data on $\langle r \rangle$, X_γ, f, and N_v are presented first, noting the assumptions involved in their derivations and usage. Criteria defining the conditions under which TIDC coarsening is expected to prevail are presented next. These criteria involve calculation of the "effective" chemical diffusion coefficient in the diffuse γ/γ' interface, $\tilde{D}_I$, as well as estimates of the interface width, δ, which ultimately enable an estimate of the transition radius, r_{trans}, below which TIDC coarsening is expected to prevail. Subsequently, published experimental data on the kinetics of γ' precipitate coarsening at twelve temperatures ranging from 773 K to 1073 K are analyzed. These analyses produce values of σ extracted from the data using the equations of the TIDC theories. For comparison σ is also calculated using the equations of the LSW theory. The results are compared with the predictions of the various theoretical approaches and discussed in their light.

II. BACKGROUND EQUATIONS

To begin, we recall the basic equations associated with the LSW and TIDC theories of particle coarsening. To simplify the presentation the equations are written in their most general form, using the parameter n as the temporal exponent. At this stage it is helpful to point out that $n = 3$ in the LSW theory, but assumes a different value in the TIDC theory satisfying the condition $2 \le n \le 3$. In the particular case of γ' coarsening in binary Ni–Al alloys $n \approx 2.4$, which is a representative value that stems from analyses[2,6,7] of γ' particle size distributions (PSDs) and experimental cumulative distribution functions in several different alloys. The temporal exponent $n = 2.4$ is used in all subsequent analysis.

The kinetics of growth of a spherical precipitate, average radius $\langle r \rangle$, at time t, is expressed by the equation

$$\langle r \rangle^n - \langle r_0 \rangle^n = kt, \qquad [1]$$

where $\langle r_0 \rangle$ is the average radius at the onset of coarsening and k is a rate constant that incorporates the thermodynamic and kinetic parameters of the alloy system. The consequences of departures from sphericity will be considered where appropriate. The variation of X_γ with t is described by the equation

$$X_\gamma - X_{\gamma e} \approx (\kappa t)^{-1/n} \qquad [2]$$

and the volume fraction, f, increases with time according to the equation

$$f = f_e - \frac{(\kappa t)^{-1/n}}{\Delta X_e}, \qquad [3]$$

where ΔX_e is the difference between the equilibrium concentrations of Al in the γ and γ' phases ($= X_{\gamma' e} - X_{\gamma e}$), and f_e is the equilibrium volume fraction of the γ' phase. Though the temporal dependence of f has been known for quite some time (with $n = 3$),[8] a particularly clear derivation can be found in a recent paper.[2] The kinetics of particle evanescence is embodied in the equation describing the temporal dependence of N_v, *i.e.*,

$$N_v = \frac{3 f_e}{4\pi\psi (kt)^{3/n}} \left\{ 1 - \frac{(\kappa t)^{-1/n}}{f_e \Delta X_e} \right\}, \qquad [4]$$

where ψ ($= \langle r^3 \rangle / \langle r \rangle^3$) depends on the particle size distribution. Equations [1] through [4] are written explicitly for spherical particles, a condition that is rarely found unless the mismatch between the γ and γ' phases is close to zero. Otherwise, the shapes of γ' precipitates are cuboidal and size dependent, becoming increasingly cube shaped as they grow.[9]

It was shown quite some time ago[10,11] that σ could be measured without having to know the value of the matrix diffusion coefficient if both k and κ could be measured independently. The most recent, and indubitably the most reliable, equation for σ is[7]

$$\sigma = \frac{\Delta X_e G''_{m\gamma e}}{2 V_{m\gamma' e} \langle z \rangle} \left(\frac{k}{\kappa} \right)^{1/n} = \frac{\Delta X_e G''_{m\gamma e}}{2 V_{m\gamma' e} \langle z \rangle} \kappa^{-1/n} k^{1/n} \qquad [5]$$

where $G''_{m\gamma e}$ is the curvature of the molar Gibbs free energy at $X_\gamma = X_{\gamma e}$, $V_{m\gamma' e}$ is the molar volume of the γ' phase evaluated at $X_{\gamma' e}$ and $\langle z \rangle = \langle r \rangle / r^*$, where r^* is a critical radius in the polydisperse array of particles such that particles with radius $r = r^*$ are stationary, *i.e.*, neither growing nor shrinking at time t; its significance is identical in both the LSW and TIDC theories. The ratio $(k/\kappa)^{1/n}$ is the capillary length in the original derivation of Eq. [5] by Calderon *et al.*[12] A brief history of the evolution of the equations relating σ and $(k/\kappa)^{1/n}$ is presented elsewhere.[7]

To calculate σ using the equations of the LSW theory we need to substitute $n = 3$ into Eqs. [1] through [5], with $\psi = 1.129$ in Eq. [4] and $\langle z \rangle = 1$ in Eq. [5]. The value of ψ obtains from the analytical equation for the PSD of the LSW theory,[3,4] which strictly speaking applies for a dispersion of particles with $f_e = 0$. Of course, $f_e \neq 0$ for any real dispersion of particles, γ' precipitates being no exception. Despite this shortcoming, there is really no other option regarding the LSW equations because the kinetics of coarsening of γ' precipitates is essentially independent of f_e for values of f_e exceeding ~ 0.08.[5,13] This is the principal drawback in using the LSW equations to estimate σ from data on coarsening. The TIDC coarsening theory does not suffer

from this misgiving because n is obtained from fitting the PSDs and their accompanying cumulative distribution functions and does not depend on f_e. For the coarsening of γ' precipitates in Ni–Al alloys the specific value $n \approx 2.4$ was obtained in precisely this way; analysis of experimental data using the TIDC coarsening theory proceeds using Eqs. [1] through [5] with $n = 2.4$, $\langle z \rangle = 0.9504$, and $\psi = 1.225$.[2,6,7]

III. THE EXTRACTION OF σ FROM THE ANALYSIS OF EXPERIMENTAL DATA

A. *Parameters Characterizing Ni-rich Ni–Al alloys*

Equation [5] is the source of all the values of σ reported in this paper. First and foremost we need to analyze experimental data to obtain values of k and κ (or more accurately $\kappa^{-1/n}$). Data on the kinetics of particle growth are the source of k, obtained from plots of $\langle r \rangle^n$ *vs* t. Values of $\kappa^{-1/n}$ can be obtained from data on the kinetics of solute depletion, augmentation of volume fraction and/or particle evanescence; there is no need to know anything about the diffusion coefficient so long as $\kappa^{-1/n}$ can be measured independently.

With measurements of k and $\kappa^{-1/n}$ in hand the temperature dependencies of ΔX_e, $G''_{m\gamma e}$ and $V_{m\gamma' e}$ must then be prescribed in order to calculate σ using Eq. [5]. In binary Ni–Al γ/γ' alloys these parameters are given by the following equations:

$$\Delta X_e = 0.19571 - 5.92586 \times 10^{-5} T - 3.37961 \times 10^{-8} T^2; \quad [6]$$

$$G''_{m\gamma e} = 203.3014 + 0.2127\ T - 6.8338 \times 10^{-5} T^2 \ \left(\text{kJ mol}^{-1}\right); \quad [7]$$

$$V_{m\gamma' e} = 6.7487 + 3.1836 \times 10^{-4} T \ \left(10^6 \text{m}^3 \text{mol}^{-1}\right). \quad [8]$$

Equation [6] is the corrected[14] version of the formula originally reported,[2] which is the source of Eqs. [7] and [8]. In Eqs. [6] through [8] T is in K. The parameters $\langle z \rangle$ and ψ depend only on n, which is itself assumed to be independent of temperature. For the sake of completeness their empirical dependencies on n are represented by the equations

$$\langle z \rangle = -0.2891 + 1.1229n - 0.3386n^2 + 0.0358n^3; \quad [9]$$

$$\psi = 4.6236 - 3.2765n + 1.0605n^2 - 0.11888n^3. \quad [10]$$

Equation [10] is also a corrected[14] version of the formula originally reported.[2] We will also refer on occasion to the γ and γ' solvus curves, $X_{\gamma e}$ and $X_{\gamma' e}$, respectively, which are represented by the equations[15]

$$X_{\gamma e} = 0.055027 \exp\left\{8.124 \times 10^{-4} T\right\}, \quad [11]$$

and

$$X_{\gamma' e} = -0.02008 + 9.653 \times 10^{-4} T - 1.313 \times 10^{-6} T^2 + 7.444 \times 10^{-10} T^3 - 1.505 \times 10^{-13} T^4. \quad [12]$$

As in Eqs. [6] through [8] T is in K.

B. *Methods of Analysis*

Whether or not the values of σ extracted from experimental data on coarsening are trustworthy depends on the nature of the data. As noted, the kinetics of at least one other variable must be measured in addition to the kinetics of particle growth in order to eliminate the need for knowledge of diffusion in the γ phase. The simplest situation involves the kinetics of solute depletion, Eq. [2]. A plot of X_γ *vs* $t^{-1/n}$ is expected to be linear in the later stages of coarsening, yielding a slope equal to $\kappa^{-1/n}$ for direct substitution into Eq. [5]. Such a plot has the added benefit of providing $X_{\gamma e}$ for the temperature of the experiment. This was the procedure originally employed[11] using magnetic analysis to measure the ferromagnetic Curie temperature, Θ_C, of aged and quenched specimens, then referring the results to a calibration curve of X_γ *vs* Θ_C to obtain data on X_γ as a function of t. Values of σ (as well as $X_{\gamma e}$) were obtained based on the assumptions that $n = 3$ (LSW coarsening kinetics) and that the Ni–Al solid solution was ideal.[10,11]

The rate constant $\kappa^{-1/n}$ can also be measured experimentally from data on either the kinetics of volume fraction augmentation (Eq. [3]) or particle evanescence (Eq. [4]). If f is measured independently Eq. [3] predicts that a plot of f *vs* $t^{-1/n}$ should be linear in the later stages of coarsening, with a slope equal to $\kappa^{-1/n}/\Delta X_e$ and intercept $f = f_e$. This procedure was used for the first time by Marsh and Chen[1] to evaluate σ at four different aging temperatures, using high-temperature X-ray diffraction methods to measure both $\langle r \rangle$ and f as functions of t. Values of σ were then obtained from the measured values of k and κ using Eq. [5], assuming LSW coarsening kinetics ($n = 3$) and an ideal Ni–Al solid solution. Marsh and Chen considered all the data on σ published up to early 1990, plotted the results *vs* T and showed that despite the scatter in the data there was an unmistakable trend for σ to decrease with increasing T.

The final option for evaluating κ experimentally is to independently measure the kinetics of particle evanescence and analyze the data using Eq. [4]. This was first attempted by Xiao and Haasen,[16] who investigated the kinetics of decomposition of a supersaturated 12.0 at. pct Al alloy aged at 773 K using high-resolution transmission electron microscopy (HRTEM). Data were obtained on $\langle r \rangle$ and N_v as functions of aging time through the nucleation and growth stages, into the coarsening regime. They used a modified version of Eq. [4] to analyze their results, once again assuming $n = 3$ and an ideal dilute Ni–Al solid solution, to extract

values of σ in good agreement with other data available at the time.

The approach of Xiao and Haasen is easiest to visualize by rewriting Eq. [4] as

$$N_v = \frac{\Phi}{t^{3/n}} - \frac{\Psi}{t^{4/n}}, \qquad [13]$$

where

$$\Phi = \frac{3f_e}{4\pi\psi k^{3/n}}, \qquad [14]$$

and

$$\Psi = \frac{-3\kappa^{-1/n}}{4\pi\psi k^{3/n}\Delta X_e}. \qquad [15]$$

Data on particle evanescence plotted as $N_v t^{3/n}$ *vs* $t^{-1/n}$ are expected to be linear, with slope $-\Psi$ and intercept Φ, while the same data plotted as $N_v t^{4/n}$ *vs* $t^{1/n}$ are also expected to be linear, with slope Φ and intercept $-\Psi$. In either case the value of $\kappa^{-1/n}$ is expressed by the equation

$$\kappa^{-1/n} = -f_e \Delta X_e \frac{\Psi}{\Phi}. \qquad [16]$$

The experimentally determined values of $\kappa^{-1/n}$ from either Eqs. [14 or [15], in conjunction with the experimentally measured value of k from a plot of $\langle r\rangle^n$ *vs* t, as prescribed by Eq. [1], can then be substituted into Eq. [5] to obtain a value of σ. A helpful byproduct of this approach is that there is no need to know anything about the PSD, since ψ is eliminated in Eq. [16]. On the other hand, the accuracy with which $\kappa^{-1/n}$is obtained also depends on the accuracy of ΔX_e and f_e. For the analyses used in this work ΔX_e is calculated using Eq. [6], and f_e is calculated from the lever rule using as inputs the overall composition of the alloy, X_0, and $X_{\gamma e}$ and $X_{\gamma' e}$ calculated using Eqs. [11] and [12]; This calculation assumes that the mass densities of the γ and γ' phases are equal, which based on the molar volumes of the γ and γ' phases is an excellent assumption.[17]

Of the three methods considered, the kinetics of particle evanescence is undoubtedly fraught with the greatest uncertainty for a variety of reasons. Equations [4] and [13] are expected to be valid only at longer aging times than Eqs. [2] and [3] due to the series expansions associated with their derivations.[2] Moreover, measurements of N_v made using techniques that involve specimens with small dimensions (foil thicknesses in TEM or HRTEM and nanometer size tips in APT for example) become increasingly error prone where accuracy is most needed, *i.e.*, at long aging times. This is because surface effects, stereological constraints, measurement of foil thickness in the case of TEM and specimen preparation issues such as preferential electrochemical or chemical attack of the phases will all adversely affect accuracy.

C. *The TIDC–LSW Transition Radius and Interface Width*

In order to proceed there are two other factors that need to be taken into consideration. The first involves the ratio of the chemical diffusion coefficient in the γ phase, $\tilde{D}_\gamma$, and the "effective" chemical diffusion coefficient in the interface region, $\tilde{D}_I$. The second factor is the previously identified width of the diffuse γ–γ' interface, δ. Knowledge of δ and the ratio $\tilde{D}_\gamma/\tilde{D}_I$ enables implementation of the criterion for the transition between TIDC and LSW coarsening kinetics, embodied in the equation

$$r_{\text{trans}} = \delta \frac{\tilde{D}_\gamma}{\tilde{D}_I}, \qquad [17]$$

where r_{trans} is a transition radius with the significance that TIDC coarsening prevails when $\langle r\rangle < r_{\text{trans}}$ and LSW coarsening prevails when $\langle r\rangle > r_{\text{trans}}$ (see Ardell and Ozolins[5] for the physical arguments apropos of this transition).

In a recent examination and evaluation by Hickman *et al.*[18] of data on coarsening of solid Sn particles in a liquid Pb-rich matrix of near eutectic composition, it was shown that an excellent estimate of the effective interface diffusion coefficient is given by the equation

$$\tilde{D}_I = 2\left\{\frac{\tilde{D}_{\gamma'}\tilde{D}_\gamma}{\tilde{D}_\gamma + \tilde{D}_{\gamma'}}\right\}, \qquad [18]$$

where $\tilde{D}_{\gamma'}$ is the chemical diffusion coefficient in the γ' phase. An updated derivation of Eq. [18] is presented in Appendix A.

There are numerous measurements of $\tilde{D}_\gamma$ and $\tilde{D}_{\gamma'}$ in Ni–Al solid solutions and Ni_3Al as functions of composition; an excellent compilation of results is found in a paper by Zhang *et al.*[19] As explained in Appendix A, the results of Watanabe *et al.*[20] were chosen to calculate reliable estimates of the temperature dependence of r_{trans} for Ni–Al solid solutions of equilibrium composition. Using their data to calculate $\tilde{D}_\gamma$ and $\tilde{D}_{\gamma'}$ at the equilibrium compositions of both phases (see Appendix A), and substituting the results into Eq. [18], leads to the temperature dependence of $\tilde{D}_\gamma/\tilde{D}_I$ displayed in Figure 1(a). The empirical equation describing the temperature dependence is

$$\frac{\tilde{D}_\gamma}{\tilde{D}_I} = 0.07481 \exp\left\{\frac{5685.86}{T}\right\}. \qquad [19]$$

The interface width, δ, was estimated from the limited sources of available experimental data, *i.e.*, the composition profiles across γ/γ' interfaces published by Plotnikov *et al.*[21,22] and a value of δ reported by Forghani *et al.*[23] Details of the analyses used to extract the data from figures published by Plotnikov *et al.* are provided in Appendix B; the analyses assume that the concentration profile across an interface is best described by a sigmoid function.[24] The results, based on limited data,

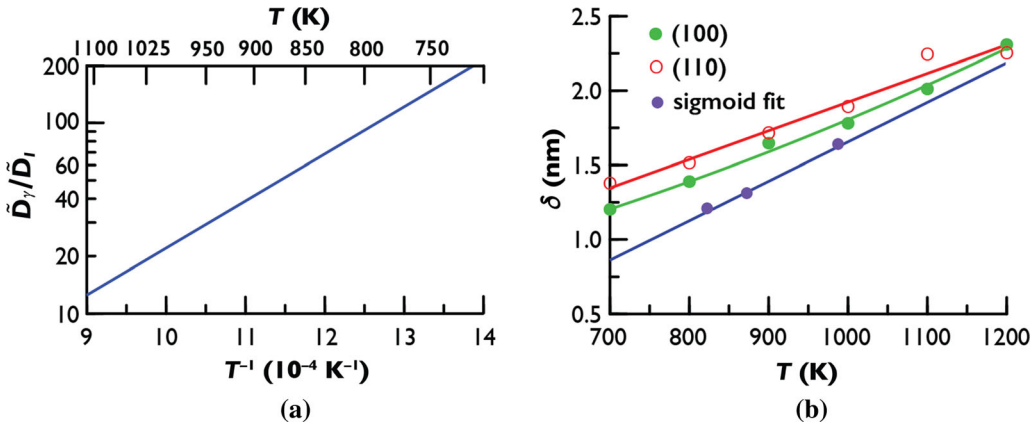

Fig. 1—(*a*) Arrhenius plot of $\tilde{D}_\gamma/\tilde{D}_I$ *vs* T^{-1} calculated from the data of Watanabe *et al.*,[20] the details of which are described in Appendix A; (*b*) The temperature dependence of the interface width, δ, obtained from analyses of sigmoid fits to the concentration profiles of Plotnikov *et al.*[21,22] and Forghani *et al.*[23] (see Appendix B). Also shown are theoretically calculated results of Woodward *et al.*[25] for the widths of the (100) and (110) γ/γ' interfaces.

indicate that δ increases with increasing temperature. This finding is supported by the theoretical calculations of Woodward *et al.*,[25] who calculated δ from their theoretically generated concentration profiles using the 10 to 90 criterion (defined in Appendix B). The graphical representation of all the information on the variation of δ with T, reported in Table BI, is shown in Figure 1(b). The equation describing the linear fit to the data is

$$\delta = -0.99513 + 2.651 \times 10^{-3} T, \qquad [20]$$

where δ is in nm and T is in K.

The calculations of Woodward *et al.*,[25] also shown in Figure 1(b), are those that agree best with δ reported in Table BI. Forghani *et al.*[23] estimated δ using the 10 to 90 criterion and found them to be about 10 pct larger than those estimated using the sigmoid-function analysis (1.79 cf. 1.63 nm). In general, the interface widths estimated using the 10 to 90 criterion are larger than those obtained using the sigmoid-function analysis. There is nothing sacrosanct about either criterion. Indeed, the application of a 1 to 99 (X_γ being 1 pct larger than $X_{\gamma e}$ and $X_{\gamma'}$ being 1 pct smaller than $X_{\gamma' e}$) criterion to an interface profile produces yet larger values of δ, which would have the benefit that δ so defined would capture the region of the interface containing the smallest concentration gradients, hence slowest rates of diffusion. This paper is not the most appropriate to argue the merits of the different criteria for estimating δ. What we can all agree to is that the sigmoid-function analysis produces the smallest values of δ, and assuredly the most conservative, and smallest, values of r_{trans}, thus providing the most stringent criterion for application of the TIDC theory to any set of data on coarsening.

IV. ANALYSES OF DATA ON THE KINETICS OF COARSENING

The data reported in this section are analyzed by all three methods described in Section III–B. They are presented in the order of the method used and afterward in chronological order. In all cases the estimates of the errors take into account only the contributions from scatter in the data used to calculate k and $\kappa^{-1/n}$, the standard errors obtained using the Microsoft Excel® macro downloaded from the link in the paper by Cantrell.[26] Errors in the other quantities required to calculate σ using Eq. [5] are not considered, even though they undoubtedly contribute to the standard deviations of the IFE. In all the data sets considered the rate constant k and its standard error, $e(k)$, are taken from the slopes of plots of $\langle r \rangle^n$ *vs* t. The following individual sub-sections consider the time dependencies of the variables X_γ, Eq. [2], f, Eq. [3] and N_v, Eq. [4]. The methods of plotting the data all yield experimental measurements of the parameter $\kappa^{-1/n}$ as well as its standard error $e(\kappa^{-1/n})$*.

*The standard error (standard deviation) of σ, $e(\sigma)$, is given by the formula $e(\sigma) = \{[e(k)]^2/n^2k^2 + [e(\kappa^{-1/n})]^2\}^{1/2}$. In the few instances of N individual measurements of σ for specific temperatures the standard error is $e(\sigma) = \{N^{-1}\Sigma[e_j(\sigma_j)]^2\}^{1/2}$, where $e_j(\sigma_j)$ is the standard error of σ_j, calculated using the equation above from the standard errors of k_j and $\kappa_j^{-1/n}$and j is an integer satisfying $1 < j < N$.

The experiments on coarsening described in the following sub-sections involve the aging of various binary Ni–Al alloys at 12 different temperatures. These aging temperatures are shown in Table I, along with the values of r_{trans} calculated using Eq. [17]. It is clear that r_{trans} decreases with increasing T, from a high of ~ 123 nm at 773 K, the lowest aging temperature used in all the work analyzed, to a low of ~ 28 nm at 1073 K, the highest aging temperature. For the most part the experimentally measured particle sizes exceeded r_{trans} in only one investigation, that of Chellman and Ardell.[27] In all the others the largest values of $\langle r \rangle$ were smaller than r_{trans}, satisfying the condition required for TIDC coarsening.

Table I. Values of r_{trans} at the 12 Aging Temperatures at Which the Data Analyzed in This Work Were Generated

T (K)	773	823	898	923	943	953	963	968	973	988	1023	1073
r_{trans} (nm)	123.40	88.86	58.26	51.43	46.77	44.68	42.72	41.79	40.89	38.36	33.31	27.69

Equations [19], [20] and ultimately [17] were used in the calculations.

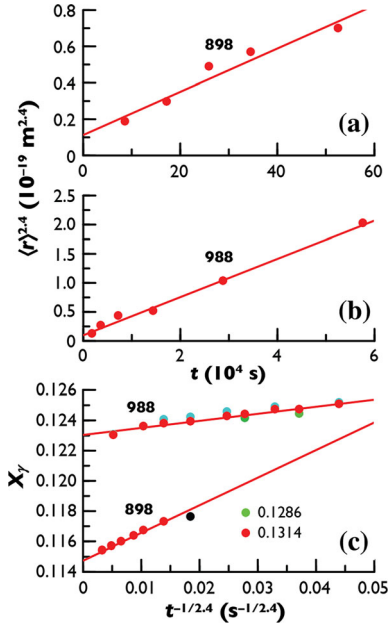

Fig. 2—The data of Ardell[11]: (*a*) and (*b*) the kinetics of particle growth plotted as $\langle r\rangle^{2.4}$ *vs* t at 898 K and 988 K, respectively; (*c*) the kinetics of solute depletion plotted as X_γ *vs* $t^{-1/2.4}$. The concentrations of Al in the alloys in (c) are indicated in the legend. The datum in black in (c) is omitted from the fit.

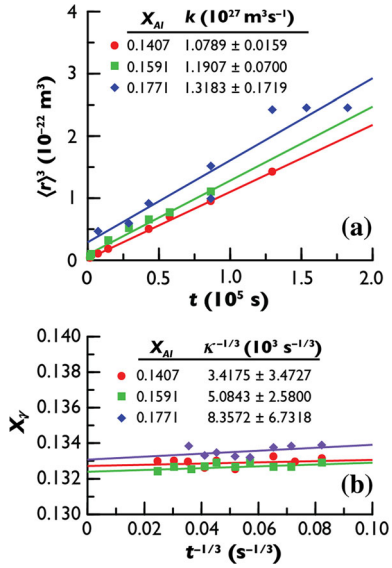

Fig. 3—The data of Chellman and Ardell[27] (*a*) the kinetics of particle growth plotted as $\langle r\rangle^3$ *vs* t; (*b*) the kinetics of solute depletion plotted as X_γ *vs* $t^{-1/3}$. The rate constants k and $\kappa^{-1/3}$ are shown for all the data.

A. *The Kinetics of Solute Depletion*

There are four contributions in this area. In chronological order they include the author's data,[11] the data of Chellman and Ardell,[27] the data of Wendt and Haasen[28], and the data of Plotnikov *et al.*[22] In the first of these investigations X_γ was measured using the aforementioned magnetic analysis, while the kinetics of particle growth was measured using dark-field TEM. The author's data and the data of Plotnikov *et al.* were previously analyzed using different values of $n = 2.432$[7] and 2.2,[2] respectively, and for that reason are re-evaluated here using $n = 2.4$. Another set of experiments by Chellman and Ardell,[27] conducted at $T = 1073$ K ($r_{trans} \approx 27.7$ nm), are the only ones that produced particle sizes overlapping the transition region from TIDC to LSW coarsening kinetics $r_{trans} \approx 27.7$ nm. These data are analyzed herein assuming LSW kinetics, with some trepidation, for reasons that will become clear later.

The author's data[11] are shown in Figure 2. An alloy containing 13.14 at. pct Al was used in most of the experiments, but an additional experiment was done on the kinetics of solute depletion using an alloy containing 12.86 at. pct Al. Data were obtained at two aging temperatures, 898 K ($r_{trans} \approx 58.3$ nm) and 988 K ($r_{trans} \approx 38.4$ nm); the largest values of $\langle r\rangle$ measured at these two temperatures were 10.4 and 16.2 nm, respectively, comfortably within the TIDC coarsening regime. The results of the two experiments on the kinetics of solute depletion at 988 K are in good agreement, the scatter in the data on the 12.86 at. pct alloy being somewhat greater than in the other alloy. The good agreement is entirely consistent with the absence of an effect of volume fraction. Considering the data on the kinetics of solute depletion at 988 K separately yields two values of σ and their standard errors. The averages of these quantities are presented in Table II. They differ slightly from those reported in Reference 7 for three reasons: 1. The smaller value of n used here; 2. The separate consideration of both sets of data on the kinetics of solute depletion in the two alloys aged at 988 K; 3. The calculation of G''_{mve} using Eq. [7] instead of the database of Ansara *et al.*[29]

Chellman and Ardell[27] measured the kinetics of particle growth and solute depletion in four binary Ni–Al alloys containing 14.07, 15.91, 17.71 and 19.30 at. pct Al aged at $T = 1073$ K. The data on the 19.30 pct alloy are not considered here due to the considerable scatter in the measurements of both $\langle r\rangle$ and X_γ. At $T = 1073$ K $r_{trans} \approx 27.7$ nm (Table I) placing the measured values of $\langle r\rangle$ in the transition region between TIDC and LSW coarsening behavior. In the 14.07 pct Al alloy ($f_e \approx$

Table II. Summary of the Parameters Used in the Calculations of σ From Analyses of the Kinetics of Solute Depletion

T (K)	ΔX_e	$G''_{m\gamma e}$(kJ mol^{-1})	$V_{m\gamma' e} \times 10^6$ (mol m^{-3})	k (m^n s^{-1})	$\kappa^{-1/n}$ (s$^{1/n}$)	σ (mJ m^{-2})	Ref.
898	0.1152	339.198	7.0346	$1.1883 \pm 0.1662 \times 10^{-25}$	0.18251 ± 0.00207	21.96 ± 1.30	11
988	0.1042	346.741	7.0632	$3.2861 \pm 0.1341 \times 10^{-24}$	0.04660 ± 0.00420	20.58 ± 1.96	11
1073	0.0932	352.849	7.0903	$1.1960 \pm 0.0978 \times 10^{-27}$	0.00768 ± 0.00424	13.96 ± 6.69	27
823	0.1240	332.066	7.0107	$1.9661 \pm 0.0503 \times 10^{-26}$	0.35009 ± 0.06646	21.05 ± 4.00	28
823	0.1240	332.066	7.0107	$9.5770 \pm 1.0119 \times 10^{-27}$	0.51481 ± 0.08403	22.94 ± 3.88	22

The temporal exponent $n = 2.4$ is used for all the data analyses except for those of Chellman and Ardell[27] (1073 K), where $n = 3$.

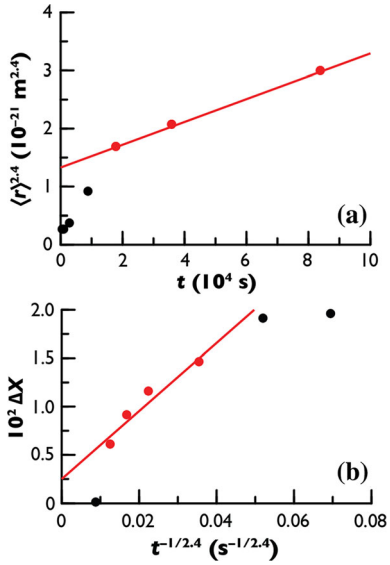

Fig. 4—The data of Wendt and Haasen[28]: (*a*) the kinetics of particle growth plotted as $\langle r \rangle^{2.4}$ *vs* t; (*b*) the kinetics of solute depletion plotted as ΔX *vs* $t^{-1/2.4}$. The data in black are omitted from the fits.

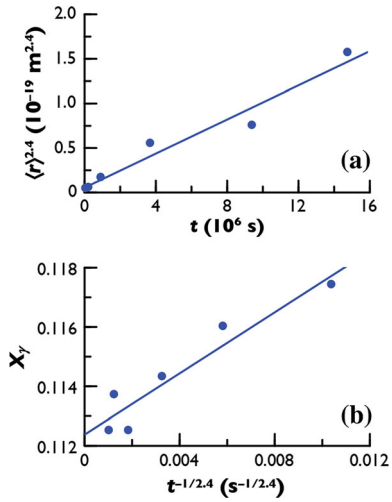

Fig. 5—The data of Plotnikov *et al.*[22]: (*a*) the kinetics of particle growth plotted as $\langle r \rangle^{2.4}$ *vs* t; (*b*) the kinetics of solute depletion plotted as X_γ *vs* $t^{-1/2.4}$.

0.098) half of the average sizes exceed r_{trans}, whereas in the 15.91 pct Al alloy ($f_e \approx 0.295$) three-fourths of the average sizes exceed r_{trans}. Only in the 17.71 pct Al alloy ($f_e \approx 0.488$) do all the particle sizes exceed r_{trans}. There is a conundrum facing the choice of temporal exponent, and as it turns out neither $n = 2.4$ nor $n = 3$ is satisfactory in the sense that it can be fully justified. The decision was taken to assume MDC coarsening kinetics, subject to the stipulation that the value of σ so obtained should not be used in final fitting of the data on σ *vs* T.

The data of Chellman and Ardell are shown in Figure 3. It is apparent in Figure 3(a) that there is a small systematic effect of initial alloy concentration, hence f_e, on the rate constant k, which increases by a factor of about 1.22. It is also evident in Figure 3(b) that the rate constant $\kappa^{-1/3}$ increases with f_e. This means that κ itself *decreases* with increasing f_e, (as reported by Chellman and Ardell[27] in Table VI of their paper). There is considerable scatter in the data on the kinetics of solute depletion, which is attributed to the necessity of quenching the aged specimens from a very high aging temperature, undoubtedly influencing the cooling rates of the individual specimens. Nevertheless, this experimental shortcoming cannot explain the unusual volume fraction dependencies of k and κ, which are simply at odds with the predictions of every theory of the influence of f_e on coarsening behavior.[30] The unexpected behavior of the rate constants notwithstanding, the equilibrium solubilities evaluated from the intercepts of the curves in Figure 3(b) are quite reasonable, *i.e.*, $X_{\gamma e} = 0.1327 \pm 0.0022$, which compares quite favorably with $X_{\gamma e} = 0.1316$ at 1073 K, calculated using Eq. [11].

The value of σ obtained by applying Eq. [5] to the data reported in Figure 3 are reported in the 3rd row of Table II. Despite the considerable misgivings articulated with the coarsening behavior reported by Chellman and Ardell and the analysis using the equations of the LSW theory, the magnitude of the IFE at 1073 K turns out to be quite reasonable, as will become evident later. The scatter in the data, which is apparent in Figure 3(b), is responsible for the very large standard deviation of the IFE reported in Table II.

Wendt and Haasen[28] investigated the early stages of γ' precipitation in a binary Ni-14 at. pct Al alloy aged at 823 K ($r_{\text{trans}} \approx 89$ nm) using atom probe tomography (ATP); their work was one of the earliest investigations using this method. The aging times ranged from 10 minutes to 23.3 hours, encompassing the nucleation stage into the early stages of the coarsening regime. They reported measurements of $\langle r \rangle$, ΔX and N_v, where

$\Delta X = X_\gamma - 0.005$, where the constant 0.005 was chosen to ensure that $\Delta X = 0$ at $t^{-1/3} = 0$. The kinetics of particle growth are shown in Figure 4(a) and the kinetics of solute depletion in Figure 4(b). The data fitted to Eq. [3] in Figure 4(b) are identical to those plotted by Wendt and Haasen, but the fitted data in Figure 4(a) include only the three longest aging times for obvious reasons. Since X_γ differs from ΔX only by a constant, the slope $\kappa^{-1/2.4}$ of the resulting linear plot of ΔX *vs* $t^{-1/2.4}$ is identical to that from a plot of X_γ *vs* $t^{-1/2.4}$ irrespective of the value of the constant. The analysis of the data produces the value of σ reported in the 4th row of Table II. It should be noted that the method of plotting the data in Figure 4(b) obviates an assessment of $X_{\gamma e}$, and in fact the combination of intercept in Figure 4(b) and the value reported by Wendt and Haasen (0.005) is quite inconsistent with the solubility limit at 823 K ($X_{\gamma e} = 0.1074$).

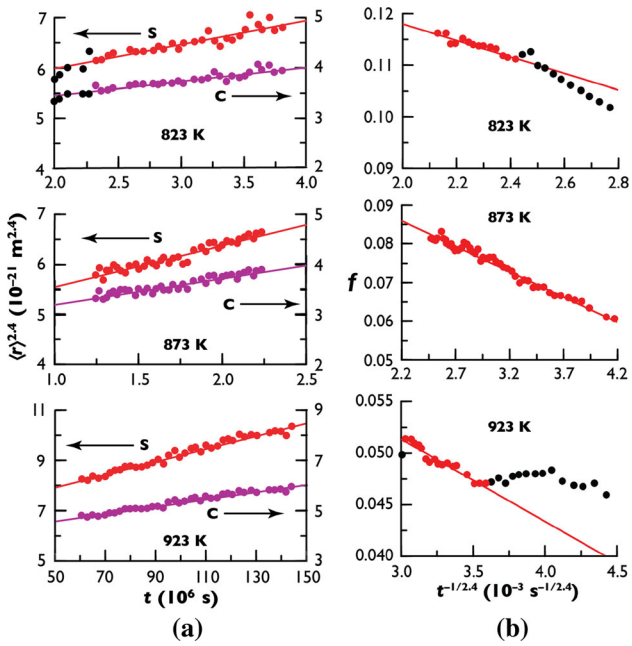

Fig. 6—(*a*) The kinetics of particle growth plotted as $\langle r \rangle^{2.4}$ *vs t*, the designations S (spherical) and C (cubic) referring to the shapes of the γ' precipitates; (*b*) the kinetics of volume fraction augmentation plotted as *f vs* $t^{-1/2.4}$. The points in black were omitted from the fits. Data of Marsh and Chen[1] from a Ni-12.5 at. pct Al alloy aged at the temperatures indicated.

The investigation of Plotnikov *et al.*[22] bears some similarities to that of Wendt and Haasen in that the aging temperature, 823 K, was the same and ATP figured prominently in the research. The main differences were the smaller alloy concentration, 12.50 at. pct Al, and much longer aging times used, the maximum value of *t* being 4096 hours. TEM and Monte Carlo simulations were also important investigative tools. Despite the much longer aging times, the largest average particle size reported was 14.59 nm (cf. 2.8 nm in Wendt and Haasen[28]), which is still much smaller than r_{trans} (~ 89 nm). A full re-analysis of the data of Plotnikov *et al.*[22] in the framework of the TIDC coarsening theory has already been published,[2] but the value of the temporal exponent in that study was $n = 2.2$, a compromise originating from analyses of the experimental cumulative distribution functions. The new analysis herein is warranted since $n = 2.4$ is used throughout in this work, The data of Plotnikov *et al.* are shown in Figure 5 and the value of σ obtained from the data are presented in the 5th row of Table II. The value of σ in Table II is smaller than that reported previously[2] because *n* is smaller, as is $G''_{m\gamma e}$, which was computed using Eq. [7] rather than directly from thermodynamic assessment of Ansara *et al.*[29] We might question whether or not the later-stage kinetics in the work Wendt and Haasen is truly representative of the coarsening regime, but the same cannot be said of the aging times used by Plotnikov *et al.* It is therefore gratifying that the rate constants obtained from the data in both investigations are in quite reasonable agreement, including the values of σ. The value of $X_{\gamma e} = 0.1124 \pm 0.0005$, obtained from Figure 5(b), is also in good agreement with the expected value of 0.1074.

The value of σ produced by the analysis of the data of Plotnikov *et al.*, 22.94 mJ m^{-2}, is smaller than the one they reported (28.55 mJ m^{-2}) from the analysis of their own data. But they assumed LWS coarsening kinetics, with $G''_{m\gamma e}$ calculated using two different thermodynamic Ni–Al databases, including the thermodynamic database of Ansara *et al.*[29] As has already been reported[2] and as emphasized here in the context of this work, not

Table III. Summary of the Parameters Derived From the Analyses of the Kinetics of Volume Fraction Augmentation Using the Temporal Exponent $n = 2.4$

T (K)	ΔX_e	f_e	$G''_{m\gamma e}$(kJ mol^{-1})	$V_{m\gamma'}$e× 10^6 (mol m^{-3})	k (10^{-27} m$^{2.4}$ s^{-1})		$\kappa^{-1/2.4}$ (s$^{1/2.4}$)	σ (mJ m^{-2})
823	0.1241	0.1420	332.066	7.0107	k_S	0.4782 ± 0.0433	1.8788 ± 0.2108	24.01 ± 2.84
					k_C	0.2781 ± 0.0253		19.16 ± 2.27
873	0.1182	0.1133	336.906	7.0266	k_S	0.8235 ± 0.0414	1.5035 ± 0.2009	23.25 ± 3.14
					k_C	0.5229 ± 0.0317		19.24 ± 2.62
923	0.1122	0.0760	341.404	7.0425	k_S	2.5633 ± 0.0744	0.9055 ± 0.0638	21.57 ± 1.54
					k_C	1.4571 ± 0.0470		17.05 ± 1.22

Data of Marsh and Chen[1] from a Ni-12.5 at. pct Al alloy. The subscripts *S* and *C* on *k* signify the assumed shape of the γ' precipitates as spheres or cubes. The values of σ in the eighth column are the IFEs based on the assumed shape.

only did Plotnikov *et al*. mis-calculate $G''_{m\gamma e}$ (269.968 cf. 332.066, see Table II), but they also included a fudge factor, 1.8308, the intent of which was to accommodate the influence of volume fraction of the kinetics of coarsening, an influence that does not, in fact, exist. Needless to say, even though σ reported by Plotnikov *et al*. is within the expected range of values, it is inarguably incorrect. A proper analysis of their data assuming MDC coarsening kinetics ($n = 3$) leads to $\sigma = 37.58 \pm 2.63$ mJ m^{-2}, which is more than 50 pct larger than their reported result and the value in Table II.

B. *The Kinetics of Volume Fraction Augmentation*

There are three investigations in this category—Marsh and Chen,[1] Kirkwood[31] and Xiao and Haasen.[16] The data from an investigation by Gröhlich *et al*.[32] can be placed in this category, but are excluded because their reported number densities, measured using two different methods, disagree significantly. The work of Marsh and Chen was quite innovative in two ways. They were the first to exploit the idea that measurements of the kinetics of particle growth and volume fraction augmentation could be combined to evaluate σ without the need to know anything about the diffusion coefficients in Ni–Al solid solutions. The second innovation involved the use of high-temperature *in situ* X-ray diffraction to measure the particle sizes and volume fractions directly as functions of aging time. We consider first the results of Marsh and Chen, then examine the results of Kirkwood and lastly those of Xiao and Haasen.

Marsh and Chen[1] investigated the precipitation of γ' in a monocrystalline Ni–Al alloy containing 12.5 at. pct Al aged at five temperatures, 823 K, 873 K, 923 K, 948 K and 973 K. The average particle sizes and volume fractions were calculated from line broadening of the $\langle 100 \rangle$ and $\langle 110 \rangle$ superlattice diffraction peaks and the integrated intensities under the peaks, respectively. Though data on the kinetics of particle growth were reported for all five aging temperatures, the kinetics of volume fraction augmentation were reported for only four: 823 K, 873 K, 923 K and 973 K. Marsh and Chen did not state specifically that the data were taken from the same specimens, but the assumption here is that they were since the time scales used in the graphical representation of their data are consistent, with the exception of the data taken at 973 K (see the abscissae in their Figures 2 and 4). Specifically, the aging times plotted in their Figures 2(e) and 4(d) cannot both be correct. Therefore, only the measurements made at 823 K, 873 K and 923 K are analyzed herein. Analyses of the Marsh-Chen data were further complicated by the very large number of data points, especially for the kinetics of particle growth. Indeed, at the shorter aging times the data are so clustered that the individual data are nearly impossible to distinguish. They were therefore treated as part of a continuous curve. The results are shown in Figure 6.

Some explanation is in order for the data in Figure 6(a). Marsh and Chen pointed out that the particle sizes estimated from line broadening of the (100) and (110) diffraction peaks were not equal, their ratios increasing with aging time. They consequently reported average sizes as either spheres (S) or cubes (C), leading to the designations in Figure 6(a). The average sizes of the particles designated S always exceeded those designated C for a given aging temperature. At all aging temperatures $\langle r \rangle < r_{\text{trans}}$, the largest reported size being $\langle r \rangle \approx 4.7$ nm at 923 K, cf. $r_{\text{trans}} \approx 51$ nm (Table I). The integrated intensities were converted to volume fractions herein as done by Marsh and Chen, *i.e*., by assuming that the ratio $I(t)/I_e = f/f_e$, where $I(t)$ and I_e are the integrated intensities at time t and thermodynamic equilibrium ($t = \infty$), respectively. To this end the data on $I(t)$ *vs* $t^{-1/2.4}$ were extrapolated to $t^{-1/2.4} = 0$ to obtain I_e for the three aging temperatures. The value of f_e at each temperature was calculated using the lever rule, after which f was calculated from the relationship $f = I(t)f_e/I_e$. The resulting plots of f *vs* $t^{-1/2.4}$, in accordance with Eq. [3], are shown in Figure 6(b), with the data used to evaluate the slopes of the curves plotted in filled red circles; the data in filled black circles were not included in the analyses. According to Eq. [3] the slopes of these curves are equal to $\kappa^{-1/2.4}/\Delta X_e$, so all that is needed to obtain $\kappa^{-1/2.4}$ is to multiply the slopes by ΔX_e, calculated using Eq. [6]. The results of all the calculations are shown in Table III where it is seen quite clearly that σ decreases with increasing T; this is consistent with the conclusion reached by Marsh and Chen.

Kirkwood[31] studied the early stages of precipitation in a Ni-13.23 at. pct Al alloy aged at 1023 K and 1073 K. Particle sizes were measured from dark-field TEM images taken using a γ' superlattice reflection. Thin wedge-shaped foils were used to measure N_v, care taken to ensure that the foil thicknesses were accurately measured from thickness extinction fringes using the best estimates of the extinction distances of the Ni–Al matrix. The volume fractions were not measured *per se*, but were calculated by the author from the measured values of $\langle r \rangle$ and N_v reported in Table I of Kirkwood's paper. The aging times in Kirkwood's investigation were not long enough to obtain reliable data on σ from the kinetics of particle evanescence, but were adequate for the analysis of data on the kinetics of volume fraction augmentation. Although the temperatures in Kirkwood's experiments were high compared to most of the others, the maximum values of $\langle r \rangle$ measured were 18 nm at 1023 K and 13 nm at 1073 K, comfortably below the values of r_{trans} at these two temperatures (33.3 and 27.7 nm, Table I).

Kirkwood observed that the γ' particles in his alloys became cuboidal in shape at $\langle r \rangle \approx 10$ nm, so to calculate f with reasonable accuracy from the tabulated values of $\langle r \rangle$ and N_v it was deemed advisable to take the change of shape of the γ' precipitates from spherical to cuboidal into account. To accommodate this shape change and its effect on the volume of a cuboidal precipitate with "radius" $r = a/2$, where a is the edge length along $\langle 100 \rangle$, the following procedure was adopted. We know that small γ' precipitates are spherical, and when the volume fraction is small enough (approximately < 0.05) they

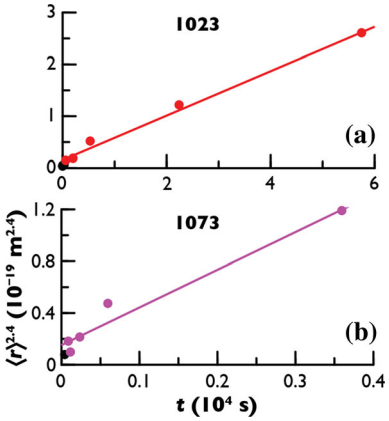

Fig. 7—The data of Kirkwood[31] on the kinetics of particle growth plotted as $\langle r \rangle^{2.4}$ *vs* t in a Ni-13.23 at. pct Al alloy aged at (*a*) 1023 K and (*b*) 1073 K. The data in black are omitted from the fits.

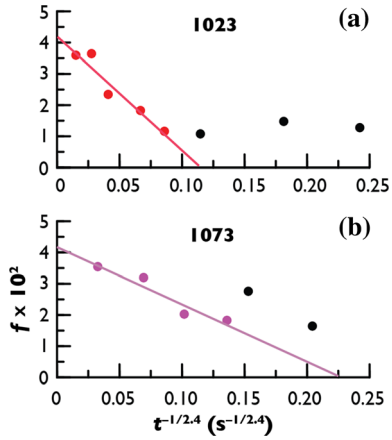

Fig. 8—The data of Kirkwood[31] on the kinetics of volume fraction augmentation plotted as f *vs* $t^{-1/2.4}$ in a Ni-13.23 at. pct Al alloy aged at (*a*) 1023 K and (*b*) 1073 K. The data in black are omitted from the fits.

have been observed to grow large enough to become nearly perfect cubes at around $a = 80$ nm[33]; they can even become concave cuboidal at larger sizes. Taking $r_{\text{cube}} = 40$ nm as the radius at which a γ' precipitate will become nearly perfectly cubic in shape,[33] with volume $= 8r_{\text{cube}}^3$, and assuming a linear relationship between r and a shape factor, S, that obeys the relationship

$$S = 0.91\left(\frac{r}{r_{\text{cube}}}\right) + 1, \qquad [21]$$

a good working expression for the volume fraction is $f = 4\pi\langle r \rangle^3 \psi S N_v/3$. It follows from Eq. [21], replacing r by $\langle r \rangle$, that $f \to 4\pi\psi\langle r \rangle^3 N_v/3$ as $\langle r \rangle \to 0$ and $f \to 8\psi\langle r \rangle^3$ as $\langle r \rangle \to \langle r \rangle_{\text{cube}}$.

The kinetics of particle growth are shown in Figure 7 and the kinetics of volume fraction augmentation are shown in Figure 8, with the results summarized in Table IV. The values of σ reported are quite reasonable, with the IFE at 1073 K slightly smaller than that at 1023 K. It is only fair to point out an inconsistency with the data of Kirkwood. The extrapolations of f to $t^{-1/2.4} = 0$ in Figure 8 lead to nearly equal values of f_e, *i.e.*, 0.0421 at 1023 K and 0.0417 at 1073 K. This raises something of a red flag because the expected values of f_e at 1073 and 1023 K are 0.0078 and 0.0599, respectively. Kirkwood calculated the quantity $8\langle r \rangle^3 N_v$ and reported them to be nearly equal at 1023 and 1073 K (see his Table I), but did not comment on this finding. The value of f_e at 1023 K is in reasonable agreement with expectation, but the value at 1073 is not. So what should we make of the observation that the IFEs from the data of Chellman and Ardell[27] and Kirkwood are in reasonably good agreement (13.96 cf. 17.04 mJ m^{-2})? It seems that the data on aging Ni–Al alloys at such high temperatures creates certain problems that might have experimental origins.

Xiao and Haasen,[16] like Wendt and Haasen before them,[28] undertook an investigation of the very early stages of γ' precipitation in a Ni-12.0 at. pct Al alloy aged at the low temperature of 773 K. The main difference between the two studies is that Xiao and Haasen measured the particle sizes and number densities using high-resolution HRTEM rather than APT. The maximum aging time in their work was 264 hours and the largest value of $\langle r \rangle$ reported was 3.4 nm, far smaller than $r_{\text{trans}} = 123.4$ nm (Table I). The aging regimes encompassed the nucleation, growth and coarsening stages, but the data on coarsening are clearly limited to the early stages of this process.

Xiao and Haasen were the first to realize that Eq. [4], or equivalently Eq. [13], could be employed to evaluate σ without the need to know anything about the diffusion coefficient. However, they were able to utilize this insight only by replacing t in Eq. [4] by $t - t_N$, where t_N is an estimated time at which the nucleation stage ended. Additionally, among all the values of N_v reported in Table I of their paper, Xiao and Haasen used what they refer to as the volume density of overcritical precipitates. Proceeding with this analysis, they reported $\sigma = 21$ mJ m^{-2}, which is certainly a quite reasonable value, but one calculated from the data using a very unrealistic model for $G''_{m\gamma e}$, *i.e.*, an infinitely dilute ideal solid solution.

After having evaluated the option of using the data of Xiao and Haasen on the kinetics of particle evanescence to estimate σ at 773 K, the following treatment using the kinetics of volume fraction augmentation was adopted. First, f was calculated using the equation $f = 4\pi\psi\langle r \rangle^3 N_v/3$ with $\langle r \rangle$ and N_v (overcritical) as input, $\psi = 1.225$, and assuming that all the γ' particles are spherical in shape. No assumptions about shape changes were necessary because largest particle size reported was only 3.1 nm and the particles were spherical in the HRTEM images. Next, the data were plotted according to Eq. [3] with t replaced by $t - t_N$ for 4 different values of t_N. Xiao and Haasen themselves chose $t_N = 40$ hours in their own analyses, but it seems reasonable to explore other options and perhaps think of t_N as representing the onset of coarsening, not necessarily the specific transition time between the nucleation and growth stages of precipitation. With these considerations in mind, the data of Xiao and Haasen are presented in Figure 9, where the kinetics of particle growth are

Table IV. Summary of the Parameters Used in the Calculations of σ From Analyses of the Kinetics of Volume Fraction Augmentation in a Ni-13.23 At. Pct Al Alloy

T (K)	ΔX_e	$G''_{m\gamma e}$(kJ mol^{-1})	$V_{m\gamma' e}\times 10^6$ (mol m^{-3})	k (m$^{2.4}$ s^{-1})	$\kappa^{-1/2.4}$ (s$^{1/2.4}$)	σ (mJ m^{-2})
1023	0.0977	349.376	7.0744	$4.2859 \pm 0.2055 \times 10^{-24}$	0.03645 ± 0.00588	17.32 ± 2.82
1073	0.0932	352.849	7.0903	$2.9214 \pm 0.3256 \times 10^{-23}$	0.01711 ± 0.00365	17.04 ± 3.92

The temporal exponent $n = 2.4$ was used for all the data analyses. Data of Kirkwood.[31].

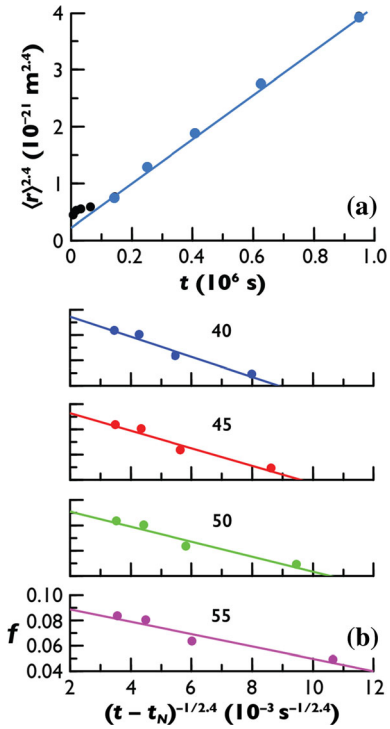

Fig. 9—The data of Xiao and Haasen[16]: (*a*) the kinetics of particle growth plotted as $\langle r\rangle^{2.4}$ *vs* t; (*b*) the kinetics of volume fraction augmentation plotted as f *vs* $(t - t_N)^{-1/2.4}$. The numbers in (b) represent the "nucleation time", t_N (h). The ordinates are identical for all four values of t_N. The data in black are omitted from the fit in (a).

Table V. Results of the Analysis of the Data of Xiao and Haasen[16] on the Kinetics of Volume Fraction Augmentation in a Ni-12.0 At. Pct Al Alloy Aged at 773 K

t_N (h)	$\kappa^{-1/2.4}$ (s$^{1/2.4}$)	f_e	σ (mJ m^{-2})
40	1.02940 ± 0.14766	0.1104 ± 0.0064	32.42 ± 4.66
45	0.90190 ± 0.14105	0.1068 ± 0.0064	28.42 ± 4.45
50	0.77084 ± 0.13456	0.1028 ± 0.0065	24.28 ± 4.24
55	0.63291 ± 0.12666	0.0985 ± 0.0066	19.93 ± 3.99

The physical parameters used in the analysis are $\Delta X_e = 0.1279$, $G''_{m\gamma e} = 326.885$ kJ mol^{-1}, $V_{m\gamma' e} = 6.9948 \times 10^{-6}$ m^3 mol^{-1}, and $k = 3.8635 \pm 0.0081 \times 10^{-27}$ m$^{2.4}$ s^{-1}.

plotted as $\langle r\rangle^{2.4}$ *vs* t, the slope of which is completely unaffected by the choice of t_N, and the kinetics of volume fraction augmentation is plotted as f *vs* $(t - t_N)^{-1/2.4}$ for four different values of t_N. None of the data published by Xiao and Haasen are omitted in Figure 9(b); only four data points remain when $t_N \geq 40$ hours.

The results of the analysis are shown in Table V. The magnitude of σ is obviously sensitive to the choice of t_N, making it difficult to specify the IFE. This is kept in mind when evaluating the temperature dependence of σ. The analysis of the kinetics of volume fragmentation augmentation also yields values of f_e from the intercepts of the plots of f *vs* $(t - t_N)^{-1/2.4}$, as per Eq. [3]. They are reported in Table V for the four different values of t_N and vary inversely with t_N from a low of 0.0985 to a high of 0.1104. The value of f_e calculated from the phase diagram is 0.1302. Considering the assumptions involved in applying the modified form of Eq. [3] to the analysis of the data, the values of f_e are regarded as reasonable.

C. *The Kinetics of Particle Evanescence*

The investigation by Hirata and Kirkwood[34] is the only one in this category. They investigated precipitation in a Ni-12.29 at. pct Al alloy aged at four different aging temperatures, 943 K, 953 K, 963 K and 968 K. Dark-field TEM using a γ' superlattice reflection was used in both works to measure the particle sizes. The largest reported value of $\langle r\rangle$ at the highest aging temperature was 7.9 nm, far smaller than $r_{\text{trans}} = 41.8$ nm at 968 K (Table I), thereby assuring that the kinetics is within the TIDC coarsening regime in all cases. Thin wedge-shaped foils were used to measure N_v, care taken to ensure that the thicknesses were accurately measured from the thickness fringes using the best estimates of the extinction distances of the Ni–Al matrix as in the work of Kirkwood.[31] Hirata and Kirkwood themselves calculated σ exclusively from the kinetics of particle growth, using published data on diffusivities, and reported values of σ that tend to increase with increasing T. All the IFEs were in reasonable agreement with results from other measurements.

To estimate the IFEs using the TIDC coarsening theory approach, the kinetics of particle growth are analyzed using the same procedures employed throughout this work, *i.e.*, by plotting $\langle r\rangle^{2.4}$ *vs* t. Based on the discussion leading to the derivations of Eqs. [13] through [16], analysis of the data on the kinetics of particle evanescence offers two measures of $\kappa^{-1/2.4}$. As stated earlier, there are 2 options for obtaining experimental values of Ψ and Φ, depending on how the data are plotted. Let Ψ_1 and Φ_1 be the slopes and intercepts of plots of $N_v t^{3/2.4}$ *vs* $t^{-1/2.4}$, and Ψ_2 and Φ_2 be the intercepts and slopes of plots of $N_v t^{4/2.4}$ *vs* $t^{3/2.4}$. If the data are self-consistent it follows that $\Phi_1 \approx \Phi_2$ and $\Psi_1 \approx$

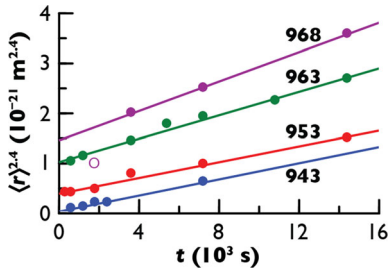

Fig. 10—The data of Hirata and Kirkwood[34] on the kinetics of growth of the γ' precipitates at the temperatures indicated in their alloy containing 12.29 at. pct Al. The data are plotted as the average radius $\langle r \rangle$ raised to the 2.4 power *vs* aging time, t. The datum indicated by the open circle (968 K) was omitted from the fit.

Ψ_2. This procedure produces 2 values of $\kappa^{-1/2.4}$, which from Eq. [16] are

$$\kappa^{-1/2.4} = -f_e \Delta X_e \frac{\Phi_1}{\Psi_1} = -f_e \Delta X_e \frac{\Phi_2}{\Psi_2}. \qquad [22]$$

The substitution of two values of $\kappa^{-1/2.4}$ into Eq. [5] yields two values of σ which should be nearly equal if the analysis is robust and self-consistent.

The data of Hirata and Kirkwood on the kinetics of particle growth are shown in Figure 10. The linearity in the plots of $\langle r \rangle^{2.4}$ *vs* t is quite good. The data on the kinetics of particle evanescence are presented in Figure 11. The scatter in the data is much larger for the specimens aged at 963 K, but otherwise the linearity at the longer aging times is as good as could be expected for both methods of plotting. The results obtained from fitting the data are shown in Table VI, the values of the pairs Φ_1:Φ_2 and Ψ_1:Ψ_2 satisfying the equalities $\Phi_1 \approx \Phi_2$ and $\Psi_1 \approx \Psi_2$ remarkably well. Using Eq. [22] to calculate the necessary eight values of $\kappa^{-1/2.4}$ (not shown), in conjunction with k from the slopes of the curves in Figure 10, substitution into Eq. [5] yields the four pairs of σ in the last column of the table. The agreement between the IFEs in each pair is excellent, the IFEs themselves decreasing with increasing temperature.

V. TEMPERATURE DEPENDENCE OF THE INTERFACIAL FREE ENERGY

The data on σ reported in Tables II through VI are shown in Figure 12, with the error bars omitted for clarity. There is a clear trend for σ to decrease with increasing T. The empirical equation, assumed linear, describing this trend is

$$\sigma = 40.868 \pm 7.898 - (0.0227 \pm 0.0085)\, T, \qquad [23]$$

where σ is in mJ m^{-2} and T is in K. The data of Xiao and Haasen[16] and Chellman and Ardell[27] are included in the figure but were not included in the fit used to produce Eq. [23]. Their inclusion in Figure 12, however, demonstrates that the values of σ obtained from their data are not very far off from the overall trend, perhaps with the exception of the datum for t_N = 40 h. The data in Figure 12(a) are compared with the results of several

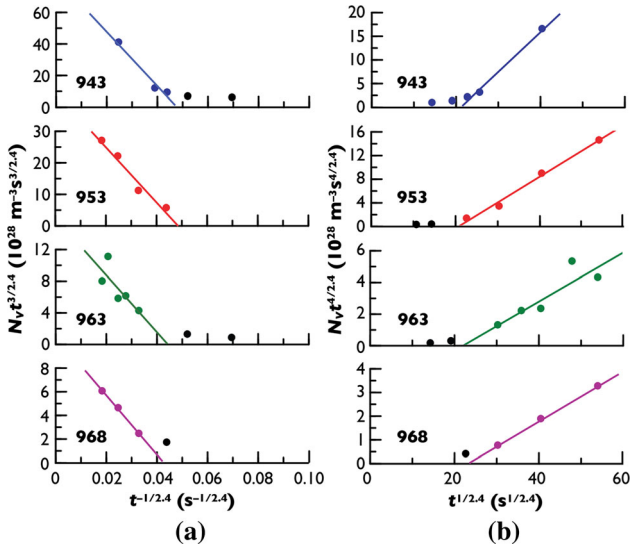

Fig. 11—The data of Hirata and Kirkwood[34] on the kinetics of particle evanescence of γ' precipitates in alloy containing 12.29 at. pct Al aged at the temperatures indicated. In (*a*) the data are plotted as $N_v t^{3/2.4}$ *vs* $t^{-1/2.4}$, whereas in (*b*) the same data are plotted as $N_v t^{4/2.4}$ *vs* $t^{1/2.4}$. Both methods of plotting are consistent with the time dependencies in Eq. [13]. In (a) the parameters Ψ_1 and Φ_1 are the slopes and intercepts, respectively, of the linear fits to the data; in (b) Φ_2 and Ψ_2 are the slopes and intercepts of the linear fits.

theoretical predictions in Figure 12(b), including those of Woodward *et al.*[25], Mao *et al.*,[35] Mishin,[36] Yang *et al.*[37], Liu *et al.*[38] and Kaptay.[17] Woodward *et al.* and Mao *et al.*[35] used first-principles atomistic theory to calculate the temperature dependencies of the ⟨100⟩, ⟨110⟩ and ⟨111⟩ IFEs in binary Ni–Al γ/γ' alloys. The curves in Figure 12(b) include the calculations of Woodward *et al.*[25] only for the (100) interface using two different cluster expansions, labeled CE1 and CE2, the results of which are very different. The curve describing the results of Mao *et al.*[35] in Figure 12(b) is their reported average value. Mishin[36] calculated the temperature dependence of σ of γ/γ' interfaces in the Ni–Al system using the capillary fluctuation method, but limited his calculations to the (100) interface. The other three theories involve detailed thermodynamic calculations in which the crystallography of the interface plays no role. Mao *et al.*[35] justify the anisotropic γ/γ' IFEs by presenting a few APT micrographs purporting to show facets on a few cuboidal-shaped precipitates; these are completely unconvincing.

The temperature dependence predicted by Eq. [23] appears to agree best with those of Kaptay[17] and Mishin,[36] which are in remarkably good agreement with each other over the temperature range 700 K to 1100 K. The temperature dependence of σ predicted by Yang *et al.*[37] is also in reasonably good agreement with the data. On evaluating the temperature dependence of σ predicted by Eq. [23], it is evident that $\sigma \approx 0$ at ~1800 K, which compares favorably with the predictions of Yang *et al.*[37] and Kaptay[17] that $\sigma = 0$ at 1893 K. According to Eq. [6] $\Delta X_e = 0$ at 1684 K. Since $\sigma = 0$ when $\Delta X_e = 0$, Eq. [5], 1684 K is another temperature at which the IFE of the γ/γ' interface should vanish. This

Table VI. Summary of the Parameters Used in the Calculations of σ From Analyses of the Kinetics of Particle Evanescence in a Ni-12.29 at. Pct Al Alloy Aged at the Four Temperatures Shown in the First Column

T (K)	ΔX_e	f_e	$G''_{m\gamma' e}$(kJ mol^{-1})	$V_{m\gamma' e}\times 10^6$ (mol m^{-3})	k (10^{-25} m$^{2.4}$ s^{-1})	#	Ψ (10^{29} s$^{3/2.4}$ m^{-3})	Φ (10^{27} s$^{4/2.4}$ m^{-3})	σ (mJ m^{-2})
943	0.1098	0.0412	343.108	7.0489	8.0872 ± 0.4143	1	1.7178 ± 0.3016	8.2030 ± 1.1115	24.34 ± 4.58
						2	1.7705 ± 0.2408	8.3871 ± 0.7868	24.54 ± 3.73
953	0.1193	0.0327	343.939	7.0521	7.8910 ± 0.5515	1	0.8741 ± 0.1222	4.2512 ± 0.3854	18.43 ± 3.09
						2	0.9189 ± 0.1137	4.3801 ± 0.2936	18.80 ± 2.90
963	0.1073	0.0240	344.757	7.0553	11.722 ± 0.5839	1	0.3603 ± 0.1628	1.5961 ± 0.4151	17.16 ± 7.83
						2	0.3420 ± 0.2014	1.5516 ± 0.4731	16.75 ± 9.93
968	0.1067	0.0196	345.161	7.0569	14.690 ± 0.3046	1	0.2493 ± 0.0097	1.0655 ± 0.0253	15.75 ± 0.75
						2	0.2461 ± 0.0102	1.0574 ± 0.0239	15.66 ± 0.78

Data of Hirata and Kirkwood.[34] The column labeled # refers to the option in Eq. [22].

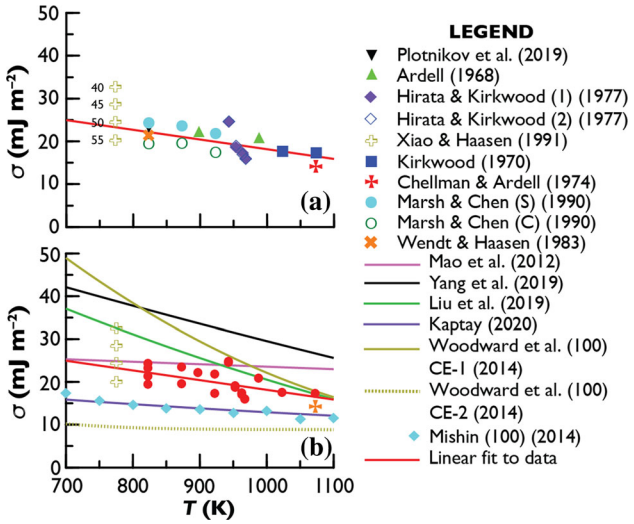

Fig. 12—(*a*) The values of σ reported in Tables II through VI plotted *vs* the aging temperature, T, of the experiments on coarsening. The numbers next to the data of Xiao and Haasen[16] represent the nucleation times, t_N in h, used in fitting their data on the kinetics of volume fraction augmentation. The data of Xiao and Haasen and Chellman and Ardell[27] were not included in the linear fit indicated by the red curve. (*b*) Illustrating the comparison between the data on σ *vs* T calculated using the TIDC theory compared with various theoretical predictions of the temperature dependence.

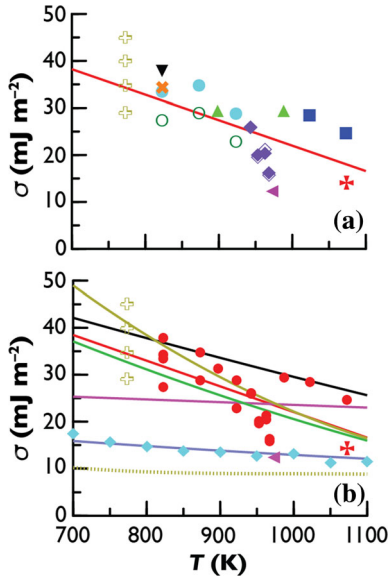

Fig. 13—(*a*) The data on σ *vs* T calculated assuming MDC coarsening, using the equations of the LSW theory ($n = 3$). (*b*) Comparison between the theoretical predictions with the data on σ. The plotting symbols are identical with those in Fig. 12, with the extra symbol, the rotated triangle, representing the datum of Zhang *et al.*[39].

makes sense physically because when the two phases have identical compositions the energy of the interface separating them should be nearly equal to zero, the only contribution being residual long-range order in the off-stoichiometric γ' phase. All three temperatures at which $\sigma = 0$ exceed the L + $\gamma \rightarrow \gamma'$ peritectic temperature (1643 K) in the Ni–Al phase diagram.[29] This finding is a consequence of the TIDC coarsening analysis that is not preordained, and is regarded as additional affirmation of the approach used in this work. It might be considered presumptuous to extrapolate Eq. [23] to $T = 0$ and expect a meaningful outcome. Nevertheless, the IFE so obtained, $\sigma \approx 41$ mJ m^{-2}, falls nearly squarely in the middle of the range of IFEs predicted theoretically, as summarized by Kaptay[17] in his Figure A3.

The interested reader will probably be curious about the outcome of analyzing the same data assuming that MDC coarsening controls the kinetics, with $n = 3$. The results of such analyses, generated using the equations of the LSW theory, are shown in Figure 13. The equation describing the temperature dependence of σ in this case is

$$\sigma = 76.7475 \pm 15.5389 - (0.05471 \pm 0.01674)\,T, \quad [24]$$

where the data of Xiao and Haasen and Chellman and Ardell are again excluded from the fit. The standard errors of the rate constants k and $\kappa^{-1/3}$ are comparable, percentage-wise, to those in the case of TIDC coarsening. The magnitudes of σ in Figure 13 are for the most part within the range of acceptable limits, and Eq. [24] is in exceptionally good agreement with the calculations of Liu *et al.*[38] However, the temperature dependence of σ is too strong. Extrapolation of Eq. [24] to the temperature at which $\sigma = 0$ leads to an unsatisfactory result,

specifically $T \approx 1403$ K, which lies well within the 2-phase $\gamma + \gamma'$ region of the phase diagram. If we demand that σ must vanish at least in the liquid region of the Ni–Al phase diagram, it is evident that this can prevail only when $n < 3$. There are certainly values of n that will enable this condition to be satisfied that have not been explored, but there is definitely an upper limit to the possibilities. Additionally, at $T = 0$ $\sigma \approx 77$ mJ m^{-2}, which close to the highest values predicted theoretically.[17]

An additional datum from the work of Zhang *et al.*[39] is included in Figure 13. They proposed a new experimental method for evaluating the γ/γ' IFE in the Ni–Al alloy system. Their method involves the preparation and subsequent analysis of data from diffusion multiples, taking advantage of a 2-phase region in a specimen annealed at 973 K. The analysis utilizes contemporary thermodynamic modeling in conjunction with what they call the KWN theory of precipitation,[40] as well as the commercial TC-PRISMA software package, which predict precipitation kinetics through the nucleation, growth and coarsening stages. Zhang *et al.* found that $\sigma = 12$ mJ m^{-2} produced the best overall fit to their data on $\langle r \rangle$ *vs* ΔX_γ (see their Figure 4). It is evident in Figure 13 that 12 mJ m^{-2} is on the low side, though it agrees quite well with the predictions of Mishin[36] and Kaptay.[17] The method of Zhang *et al.* seems quite promising. However, it depends on the applicability of MDC precipitation kinetics, including LSW coarsening kinetics in the late stages. The method of Zhang *et al.* does not appear to be readily amenable to modification by trans-interface diffusion-controlled kinetics. In this context it seems worth mentioning that all the values of $\langle r \rangle$ reported by Zhang *et al.* are smaller than $r_{\text{trans}} \approx 40.9$ nm at 973 K (Table I), so that TIDC coarsening should prevail.

In closing, there is a very important point that must be made in the context of the analysis of data on the kinetics of evanescence. Conventional wisdom asserts that $N_v \propto t^{-1}$, in direct contradiction to Eq. [4] with $n = 3$. It was shown quite some time ago[41] that Eq. [4] is correct. Sometime later the relationship between N_v and t was generalized and shown to successfully describe the kinetics of particle evanescence for a variety of different coarsening problems.[42] However, until the current investigation of the temperature dependence of the IFE, Eq. [4] had never been used successfully to obtain robust quantitative data on σ, the early attempt by Xiao and Haasen[16] notwithstanding. The analyses of the data of Hirata and Kirkwood[34] on the kinetics of particle evanescence during coarsening yield perfectly reasonable values of σ, which are entirely consistent with the trend reported in Figure 12. If this observation does not disabuse the community of the canard that $N_v \propto t^{-1}$during coarsening, it is highly likely that nothing ever will. The persistence with which the relationship $N_v \propto t^{-1}$ is promulgated in the literature is most disheartening, speaks to its stubborn acceptance and encourages the uninitiated researcher to believe what is ultimately a misconception that has approached nearly theological conviction. The relationship $N_v \propto t^{-1}$ during coarsening perhaps has its origins in the original paper by Lifshitz and Slyozov,[3] whose derivation explicitly assumed constancy of volume fraction. Of course, if $f = f_e$ then, and only then, is $N_v \propto t^{-1}$. But f can *never* be constant during coarsening, as clearly shown in Reference 2, so the time has truly come to send this antiquated and patently incorrect relationship to its grave, once and for all.

VI. SUMMARY AND CONCLUSIONS

- The temperature dependencies of several physical and thermodynamic parameters are presented as a prelude to calculating the γ/γ' interfacial free energies as a function of temperature. These include empirical equations describing the dependencies on T of ΔX_e (Eq. [6]), $G''_{m\gamma e}$ (Eq. [7]), $V_{m\gamma'}$e. (Eq. [8]), and $X_{\gamma e}$ (Eq. [11]).
- A transition radius, r_{trans}, is calculated as a function of temperature. TIDC coarsening is expected to prevail when $\langle r \rangle < r_{\text{trans}}$, and LSW coarsening is expected to prevail when $\langle r \rangle > r_{\text{trans}}$. The transition radius depends on the product $\delta \tilde{D}_\gamma / \tilde{D}_I$ (Eq. [17]). Using published data on chemical diffusion in Ni–Al γ/γ' alloys, $\tilde{D}_I$ in the diffuse γ/γ' interface is estimated quantitatively for the first time; it is given by Eqs. [18] and [19]. Using data in the literature, the width δ of the diffuse γ/γ' interface was calculated as a function of temperature, thereby ultimately enabling an estimate of the temperature dependence of r_{trans} (Table I). With one exception, all the data analyzed on the kinetics of coarsening of γ' precipitates in Ni–Al alloys satisfy $\langle r \rangle < r_{\text{trans}}$, thereby justifying the applicability of the TIDC theory.
- The interfacial free energy of the γ/γ' interface was calculated using Eq. [5] with input from the rate constants k and $\kappa^{-1/n}$, with temporal exponents $n = 2.4$ (TIDC) and $n = 3$ (LSW). The rate constants k were evaluated exclusively from plots of $\langle r \rangle^n$ *vs* t. The rate constants $\kappa^{-1/n}$ were obtained from analyses of the kinetics of solute depletion, the kinetics of volume fraction augmentation, and the kinetics of particle evanescence. The last of these methods would not be possible if $N_v \propto t^{-1}$, as is commonly assumed.
- The interfacial free energy of the γ/γ' interface decreases with increasing temperature. The temperature dependence of σ estimated from data on coarsening using the equations of the TIDC theory ($n = 2.4$) is described by the empirical equation $\sigma = 40.868 - 0.0227T$. This equation predicts that $\sigma = 0$ at ~1800 K, which is clearly within the liquid region of the Ni–Al phase diagram, as it should be. On the other hand, the values of σ estimated using the equations of the LSW theory ($n = 3$) decrease with temperature much more rapidly, as described by the equation $\sigma = 76.747 - 0.0547T$. This equation predicts that $\sigma = 0$ at ~1403 K. This is a physically unsatisfactory result because 1403 K lies well within the two-phase $\gamma + \gamma'$ region of the phase diagram,

wherein the two phases cannot possibly coexist with an interfacial free energy equal to zero.
- It is concluded that the TIDC theory of coarsening provides the best and most complete quantitative description of the early stage of coarsening behavior of γ' precipitates in binary Ni–Al alloys, *i.e.*, the stage for which $\langle r \rangle < r_{\text{trans}}$. This sweeping statement includes every aspect of coarsening behavior, from the kinetics of every measureable quantity ($\langle r \rangle$, X_γ, f and N_v), in conjunction with the temporal exponent $n = 2.4$ (and more importantly $n \neq 3$), the particle size and experimental cumulative distribution functions, and, as demonstrated herein, the temperature dependence of the interfacial free energy σ.

ACKNOWLEDGMENTS

The author is grateful to Professor Yuri Mishin, Physics and Astronomy Department, George Mason University, for his insight in enabling a quantitative estimate of the chemical diffusion coefficient in a diffuse interface. He is also to be thanked for sharing his knowledge of the atomic structure of the coherent γ/γ' interface.

CONFLICT OF INTEREST The corresponding author states that there is no conflict of interest.

APPENDIX A: THE INTERFACE DIFFUSION COEFFICIENT

The purpose of this appendix is to estimate the coefficient of chemical diffusion in the diffuse γ/γ' interface. The approach mimics that used in a recent paper by Hickman *et al.*[18] In that paper the variation of any property $P(x)$ that varies with directional coordinate x across a diffuse interface is described by the equation

$$P(x) = \frac{P_{\gamma'} - P_\gamma}{2}\left\{\tanh\left[\frac{2x}{w}\right] + 1\right\} + P_\gamma, \qquad [A1]$$

which is specifically written here expressly for the γ and γ' phases flanking the interface. In Eq. [A1] $P_{\gamma'}$ and P_γ represent the far-field values of any property of the γ' and γ phases, respectively, and w is related to the width, δ, of the interface. Since $\{1 + \tanh(x/2w)\}/2 = 1/\{1 + \exp(-x/w)\}$ we can immediately rewrite Eq. [A1] as

$$\frac{P(x) - P_\gamma}{P_{\gamma'} - P_\gamma} = \frac{1}{1 + e^{-x/w}}, \qquad [A2]$$

which is equivalent to the sigmoid function used to investigate interface properties of diffuse interfaces in different alloys,[24] with w^{-1} replacing the parameter η.

The average value of $P(x)$ through the interface region, $\langle P \rangle$, is readily calculated[18] using the formula $\langle P \rangle = \delta^{-1} \int_{-\delta/2}^{\delta/2} P(x)\, dx$. On performing the integration using Eq. [A1] we obtain the general result

$$\langle P \rangle = \frac{P_{\gamma'} + P_\gamma}{2}. \qquad [A3]$$

As an example, Eq. [A3] tells us that the average concentration of Al in the interface region, is the expected result $\langle X_{Al} \rangle = (X_\gamma + X_{\gamma'})/2$, where $X_{Al} = X_{Al}(x)$ is the general atom fraction of Al across the interface. As in the paper by Hickman *et al.*,[18] the property of interest in the diffusion problem is, following Crank,[43] $\tilde{D}^{-1}(x)$, which on application of Eq. [A3] leads to the result

$$\left\langle \frac{1}{\tilde{D}} \right\rangle = \frac{1}{2}\left(\frac{1}{\tilde{D}_{\gamma'}} + \frac{1}{\tilde{D}_\gamma}\right). \qquad [A4]$$

On writing $\tilde{D}_I = \langle 1/\tilde{D} \rangle^{-1}$ we obtain the final result

$$\frac{1}{\tilde{D}_I} = \frac{1}{2}\left(\frac{1}{\tilde{D}_{\gamma'}} + \frac{1}{\tilde{D}_\gamma}\right), \qquad [A5]$$

which leads directly to Eq. [18].

As stated in the main text, the data of Watanabe *et al.*[20] on chemical diffusion in the γ and γ' phases were chosen for the estimation of $\tilde{D}_I$. The reason for this choice is that the experiments were done using specimens and methods of analysis, analytical electron microscopy (AEM) and electron probe microanalysis (EPMA), that provided self-consistent data on chemical diffusion in both phases over a range of temperatures and compositions from 1073 K to 1473 K. The lowest temperature in their work coincides with the highest temperature used in all the coarsening experiments, thereby obviating the need for excessively large extrapolations of data.

The results of Watanabe *et al.* are reproduced in Figure A1. The data measured using AEM and EPMA are presented without distinction in Figure A1(a) simply because there is no need to distinguish them. The plots

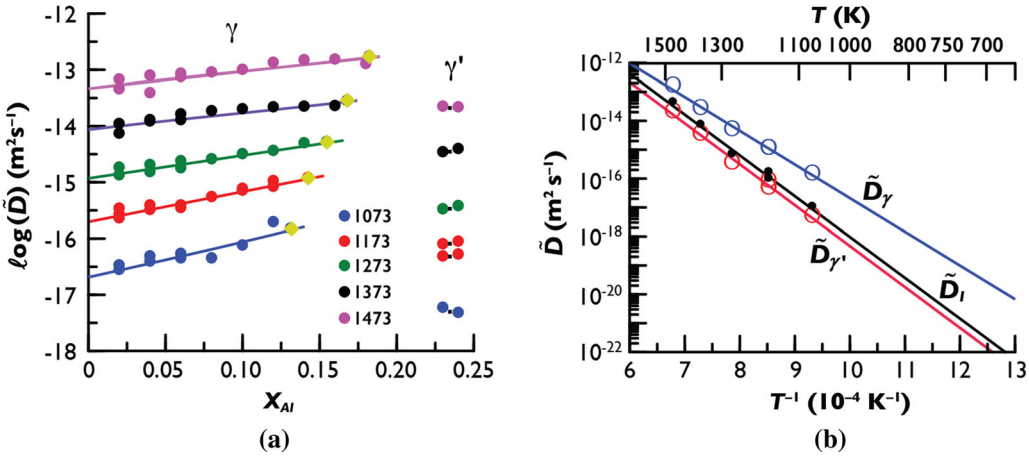

Fig. A1—(*a*) The data of Watanabe *et al.*[20] plotted as the logarithm of the chemical diffusion coefficient, $\tilde{D}$, *vs* atom fraction of Al, X_{Al}. The filled diamond symbols represent the values of $\tilde{D}_\gamma$ at the equilibrium solubilities of Al in the γ phase; (*b*) Arrhenius plots illustrating the temperature dependencies of the chemical diffusion coefficients in the γ and γ' phases $\tilde{D}_\gamma$ and $\tilde{D}_{\gamma'}$, respectively) and the chemical diffusion coefficient in the interface, $\tilde{D}_I$, calculated from Eq. [A5].

of $\ell og(\tilde{D}_\gamma)$ *vs* X_{Al} for the γ phase at each temperature were fitted by a linear equation, which was then used to calculate the value of $\tilde{D}_\gamma$ at $X_{\gamma e}$. The data on X_{Al} in the γ' phase were taken as independent of composition over the small range 22.5 to 23.0 at. pct Al seen in Figure A1(a), the values of $\ell og(\tilde{D}_{\gamma'})$ taken as the average of the two data at each temperature in Figure A1(a). Equation [A5] was then used to calculate $\tilde{D}_I$, leading to the results shown in Figure A1(b). As expected, $\tilde{D}_I$ is dominated by $\tilde{D}_{\gamma'}$, the chemical diffusion in the ordered phase. At the lower temperatures of the coarsening experiments diffusion in the ordered γ' phase is about 2 orders of magnitude slower than in the disordered γ phase.

APPENDIX B: THE INTERFACE WIDTH

The interface width, δ, is estimated using the limited sources of available experimental data, namely the composition profiles across γ/γ' interfaces published by Plotnikov *et al.*[21,22] and a value of δ reported by Forghani *et al.*[23] Plotnikov *et al.* used the distances between the two values of X_{Al} within 10 pct of the concentration in the γ phase and 90 pct of the concentration in the γ' phase (the 10 to 90 method) as the measure of δ. Forghani *et al.*, on the other hand, followed a procedure that involves fitting the sigmoid function, Eq. [A2], to the concentration profile itself to evaluate δ from the relationship $\delta = 4w$.[24] For the sake of consistency, the concentration profiles corresponding to the longest aging times used in the papers of Plotnikov *et al.*[21,22] were also analyzed using the sigmoid-function approach. To implement this approach we let the property $P(x) = X_{Al} = X_{Al}(x)$ in Eq. [A2], with $P_\gamma = X_\gamma$ and $P_{\gamma'} = X_{\gamma'}$, and rewrite it in the form

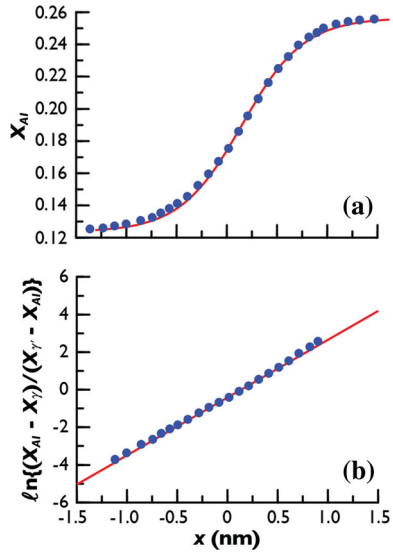

Fig. B1—(*a*) Concentration profile across the interface of a binary Ni-12.5 at. pct Al alloy aged for 1 h at 873 K. Data of Plotnikov *et al.*[21]; (*b*) Most of the data in (a) plotted as $\ell n\{(X_{Al} - X_\gamma)/(X_{\gamma'} - X_{Al})\}$ *vs* the distance coordinate x.

$$\ell n\left\{\frac{X_{Al} - X_\gamma}{X_{\gamma'} - X_{Al}}\right\} = \frac{x}{w}. \qquad [B1]$$

According to Eq. [B1] a plot of $\ell n\{(X_{Al} - X_\gamma)/(X_{\gamma'} - X_{Al})\}$ *vs* x should be linear, with slope w^{-1}. The interface width is then obtained from the relationship $\delta = 4w$.[24] In practice the scatter in experimental concentration profiles is such that linearity in a plot of $\ell n\{(X_{Al} - X_\gamma)/(X_{\gamma'} - X_{Al})\}$ *vs* x is unusual over the entire range of data, so for the most part the usable data encompass a range of X_{Al} comfortably within the interface region. It

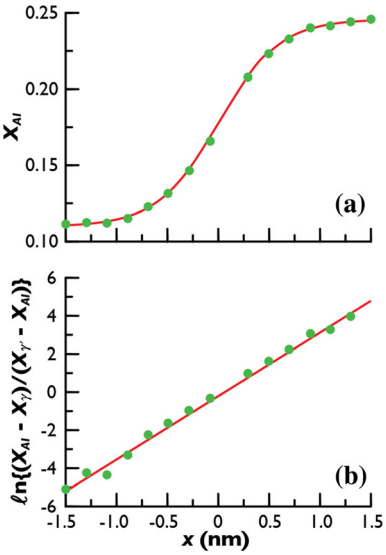

Fig. B2—(*a*) Concentration profile across the interface of a binary Ni-12.5 at. pct Al alloy aged for 4096 h at 823 K. Data of Plotnikov *et al.*[22]; (*b*) Most of the data in (a) plotted as $\ell n\{(X_{Al} - X_\gamma)/(X_{\gamma'} - X_{Al})\}$ *vs* the distance coordinate x.

Table BI. Presentation of the Parameters Used in the Analyses of the Data in Figs. B1 and B2

T (K)	X_γ	$X_{\gamma'}$	w (nm)	δ (nm)
823	0.1098	0.2459	0.300	1.20
873	0.1236	0.2566	0.325	1.30
988	—	—	0.407	1.63

Data of Plotnikov *et al.*[21,22]. The data of Forghani *et al.*[23] are included for the sake of completeness (they did not report the data on X_γ and $X_{\gamma'}$ used in their analysis).

is also necessary to evaluate the goodness of fit by adjusting X_γ and $X_{\gamma'}$ slightly, noting that they are not necessarily their thermodynamic equilibrium values, in part due to the influence of capillarity. With these limitations in mind, the data of Plotnikov *et al.*[21,22] are displayed in Figures B1 and B2**. A summary of the results of the analyses of the data is presented in Table BI, along with the datum of Forghani *et al.*,[23] who used the sigmoid-based analysis to obtain the width γ/γ' interface their Ni-19 at. pct Al alloy aged at 988 K.

It is clear from the data in Table BI that δ is temperature dependent, increasing with increasing T. This trend was pointed out by Forghani *et al.*[23] and is predicted theoretically by Woodward *et al.*[25] specifically for the γ/γ' interface in Ni–Al alloys. The results of Woodward *et al.*[25] for the (100) and (110) interfaces, calculated using the cluster expansion designated CE1, agree most closely with those from the analyses of the concentration profiles; they are shown in Figure 1(b) in the main text along with the 3 experimentally measured value of δ in Table BI.

**The data of Plotnikov et al.[21] on the 12.5 pct Al alloy aged at 873 K are clustered together within the precipitate and matrix regions to such an extent that the individual points cannot be distinguished. This is not the case for the data within the interface region. Despite this limitation, there was no problem choosing representative data in the regions flanking the diffuse interface by treating the clustered data as continuous curves.

ABBREVIATIONS

σ	Interfacial free energy
T	Absolute temperature
n	Temporal exponent
r	Radius of a precipitate
$\langle r \rangle$	Average radius of precipitates in a polydisperse assembly
$\langle r_0 \rangle$	Average radius at the onset of coarsening
r_{trans}	The radius at the transition from TIDC to MDC coarsening
γ	The Ni–Al solid solution phase
γ'	The ordered Ni_3Al phase
t	Aging time
t_N	Aging time representing the end of the nucleation stage of precipitation
X_γ	The concentration of Al in the γ phase
$X_{\gamma e}$	The concentration of Al in the γ phase at thermodynamic equilibrium
$X_{\gamma'}$	The concentration, atom fraction, of Al in the γ' phase
$X_{\gamma' e}$	The concentration of Al in the γ' phase at thermodynamic equilibrium
X_{Al}	Generalized concentration of Al in equations and figures involving both the γ and γ' phases
X_0	The concentration of Al in the alloy
ΔX	X_γ—Constant, used in only one instance
ΔX_e	$X_{\gamma' e} - X_{\gamma e}$
f	The volume fraction of the γ' phase in the alloy
f_e	The thermodynamic equilibrium volume fraction of the γ' phase
N_v	The number of γ' precipitates per unit volume in the alloy
$\tilde{D}_I$	The chemical diffusion coefficient in the diffuse γ/γ' interface
$\tilde{D}_\gamma$	The chemical diffusion coefficient in the γ phase
$\tilde{D}_{\gamma'}$	The chemical diffusion coefficient in the γ' phase
$G''_{m\gamma e}$	The curvature of the molar Gibbs free energy at $X_\gamma = X_{\gamma e}$
$V_{m\gamma' e}$	The molar volume of the γ' phase evaluated at $X_{\gamma'} = X_{\gamma' e}$
k	Rate constant for growth of the average particle during coarsening
κ	Rate constant for the kinetics of solute depletion during coarsening
$e(q)$	Standard error of the quantity q ($= \sigma, k, \kappa^{-1/n}$)
N	Number of individual measurements of q for a specific aging temperature
r^*	Critical radius in the polydisperse assembly at which $dr/dt = 0$
z	Scaled radius, $= r/r^*$
$\langle z \rangle$	$\langle r \rangle / r^*$, which depends on n *via* the PSD

ψ	The ratio $\langle r^3\rangle/\langle r\rangle^3$; $\langle z\rangle$ and ψ both depend on the particle size distribution
Θ_C	Ferromagnetic Curie temperature
Φ ,Ψ	Intercept or slope in the equation for the kinetics of particle evanescence, depending on how the data are plotted
δ	The width of the diffuse γ/γ' interface
$I(t)$	The time-dependent integrated X-ray intensity under a superlattice peak
I_e	The integrated x-ray intensity under a superlattice peak at thermodynamic equilibrium
a	Edge length of a cuboidal particle
r_{cube}	The ''effective'' radius of a perfectly cube-shaped γ' particle; $r_{\text{cube}} = a/2$
S	Shape factor that determines the effective radius of a cuboidal particle of edge length a
x	Distance coordinate across the γ/γ' interface
$P(x)$	General representation of any property that varies with x across the γ/γ' interface
P_γ, $P_{\gamma'}$	The far-field constant values of $P(x)$ in the γ and γ' phases, respectively
w	A parameter proportional to the interface width
η	w^{-1}

REFERENCES

1. C. Marsh and H. Chen: *Acta Metall. Mater.*, 1990, vol. 38, pp. 2287–98.
2. A.J. Ardell: *J. Mater. Sci.*, 2020, vol. 55, pp. 14588–4610.
3. I.M. Lifshitz and V.V. Slyozov: *J. Phys. Chem. Solids*, 1961, vol. 19, pp. 35–50.
4. C. Wagner: *Zeitschrift Für Elektrochemie*, 1961, vol. 65, pp. 581–91.
5. A.J. Ardell and V. Ozolins: *Nat. Mater.*, 2005, vol. 4, pp. 309–16.
6. A.J. Ardell: *Acta Mater.*, 2010, vol. 58, pp. 4325–31.
7. A.J. Ardell: *J. Mater. Sci.*, 2011, vol. 46, pp. 4832–49.
8. A.J. Ardell: in *Mechanism of Phase Transformations in Crystalline Solids*, Inst. of Metals Monograph & Report Series 33, London, UK, 1969, pp. 111–16.
9. A.J. Ardell and R.B. Nicholson: *Acta Metall.*, 1966, vol. 14, pp. 1295–1309.
10. A.J. Ardell: *Acta Metall.*, 1967, vol. 15, pp. 1772–75.
11. A.J. Ardell: *Acta Metall.*, 1968, vol. 16, pp. 511–16.
12. H.A. Calderon, P.W. Voorhees, J.L. Murray, and G. Kostorz: *Acta Metall. Mater.*, 1994, vol. 42, pp. 991–1000.
13. A.J. Ardell: *Scr. Metall. Mater.*, 1990, vol. 24, pp. 343–46.
14. A.J. Ardell: *J. Mater. Sci.*, 2020, vol. 55, p. 16860.
15. A.J. Ardell: *Philos. Mag.*, 2014, vol. 94, pp. 2101–30.
16. S.Q. Xiao and P. Haasen: *Acta Metall. Mater.*, 1991, vol. 39, pp. 651–59.
17. G. Kaptay: *Adv. Colloid Interface Sci.*, 2020, vol. 283, p. 102212.
18. J.F. Hickman, Y. Mishin, V. Ozolins, and A.J. Ardell: *Phys. Rev. Mater.*, 2021, vol. 5, pp. 1–17.
19. L. Zhang, Y. Du, Q. Chen, I. Steinbach, and B. Huang: *Int. J. Mater. Res.*, 2010, vol. 101, pp. 1461–75.
20. M. Watanabe, Z. Horita, T. Sano, and M. Nemoto: *Acta Metall. Mater.*, 1994, vol. 42, pp. 3389–96.
21. E.Y. Plotnikov, Z.G. Mao, R.D. Noebe, and D.N. Seidman: *Scr. Mater.*, 2014, vol. 70, pp. 51–54.
22. E.Y. Plotnikov, Z. Mao, S. Il Baik, M. Yildirim, Y. Li, D. Cecchetti, R.D. Noebe, G. Martin, and D.N. Seidman: *Acta Mater.*, 2019, vol. 171, pp. 306–33.
23. F. Forghani, J.C. Han, J. Moon, R. Abbaschian, C.G. Park, H.S. Kim, and M. Nili-Ahmadabadi: *J. Alloys Compd.*, 2019, vol. 777, pp. 1222–33.
24. A.J. Ardell: *Scr. Mater.*, 2012, vol. 66, pp. 423–26.
25. C. Woodward, A. Van De Walle, M. Asta, and D.R. Trinkle: *Acta Mater.*, 2014, vol. 75, pp. 60–70.
26. C.A. Cantrell: *Atmos. Chem. Phys.*, 2008, vol. 8, pp. 5477–87.
27. D.J. Chellman and A.J. Ardell: *Acta Metall.*, 1974, vol. 22, pp. 577–88.
28. H. Wendt and P. Haasen: *Acta Metall.*, 1983, vol. 31, pp. 1649–59.
29. I. Ansara, N. Dupin, H.L. Lukas, and B. Sundman: *J. Alloys Compd.*, 1997, vol. 247, pp. 20–30.
30. A. Baldan: *J. Mater. Sci.*, 2002, vol. 37, pp. 2171–202.
31. D.H. Kirkwood: *Acta Metall.*, 1970, vol. 18, pp. 563–70.
32. M. Gröhlich, P. Haasen, and G. Frommeyer: *Scr. Metall.*, 1982, vol. 16, pp. 367–70.
33. A.J. Ardell and D.M. Kim: *Phase Transform. Evol. Mater.*, P.E.A. Turchi and A. Gonis, eds., The Minerals, Metals & Materials Society, Warrendale, 2000, pp. 309–20.
34. T. Hirata and D.H. Kirkwood: *Acta Metall.*, 1977, vol. 25, pp. 1425–34.
35. Z.G. Mao, C. Booth-Morrison, E. Plotnikov, and D.N. Seidman: *J. Mater. Sci.*, 2012, vol. 47, pp. 7653–59.
36. Y. Mishin: *Model. Simul. Mater. Sci. Eng.*, 2014, vol. 22, art. no. 045001.
37. S. Yang, J. Zhong, J. Wang, L. Zhang, and G. Kaptay: *J. Mater. Sci.*, 2019, vol. 54, pp. 10297–10311.
38. Y. Liu, S. Liu, Y. Du, Y. Peng, C. Zhang, and S. Yao: *Calphad Comput. Coupling Phase Diagrams Thermochem.*, 2019, vol. 65, pp. 225–31.
39. Q. Zhang, S.K. Makineni, J.E. Allison, and J.C. Zhao: *Scr. Mater.*, 2019, vol. 160, pp. 70–74.
40. R. Kampmann and R. Wagner: *in Decomposition of Alloys: The Early Stages,* P. Haasen, V. Gerold, M.F. Ashby and R. Wagner, eds., Pergamon Press, Oxford, 1984, pp. 91–103.
41. A.J. Ardell: *Phase Transform. '87*, G. Lorimer, ed., The Inst. of Metals, London, 1988, pp. 35–40.
42. A.J. Ardell: *Mater. Sci. Eng. A*, 1997, vol. 238, pp. 108–20.
43. J. Crank: *The Mathematics of Diffusion*, 2nd ed., Oxford University Press, London, 1975, p. 273.